11-10-2003

Measurement of the Open-charm Contribution to the Diffractive Proton Structure Function

S. Chekanov
Argonne National Laboratory

M. Derrick
Argonne National Laboratory

D. Krakauer
Argonne National Laboratory

J. H. Loizides
Argonne National Laboratory

S. Magill
Argonne National Laboratory

See next page for additional authors

DESY–03–094
July 2003

Measurement of the open-charm contribution to the diffractive proton structure function

ZEUS Collaboration

Abstract

Production of $D^{*\pm}(2010)$ mesons in diffractive deep inelastic scattering has been measured with the ZEUS detector at HERA using an integrated luminosity of 82 pb^{-1}. Diffractive events were identified by the presence of a large rapidity gap in the final state. Differential cross sections have been measured in the kinematic region $1.5 < Q^2 < 200\,\mathrm{GeV}^2$, $0.02 < y < 0.7$, $x_{I\!P} < 0.035$, $\beta < 0.8$, $p_T(D^{*\pm}) > 1.5\,\mathrm{GeV}$ and $|\eta(D^{*\pm})| < 1.5$. The measured cross sections are compared to theoretical predictions. The results are presented in terms of the open-charm contribution to the diffractive proton structure function. The data demonstrate a strong sensitivity to the diffractive parton densities.

The ZEUS Collaboration

S. Chekanov, M. Derrick, D. Krakauer, J.H. Loizides[1], S. Magill, B. Musgrave, J. Repond, R. Yoshida
Argonne National Laboratory, Argonne, Illinois 60439-4815 [n]

M.C.K. Mattingly
Andrews University, Berrien Springs, Michigan 49104-0380

P. Antonioli, G. Bari, M. Basile, L. Bellagamba, D. Boscherini, A. Bruni, G. Bruni, G. Cara Romeo, L. Cifarelli, F. Cindolo, A. Contin, M. Corradi, S. De Pasquale, P. Giusti, G. Iacobucci, A. Margotti, R. Nania, F. Palmonari, A. Pesci, G. Sartorelli, A. Zichichi
University and INFN Bologna, Bologna, Italy [e]

G. Aghuzumtsyan, D. Bartsch, I. Brock, S. Goers, H. Hartmann, E. Hilger, P. Irrgang, H.-P. Jakob, A. Kappes[2], U.F. Katz[2], O. Kind, U. Meyer, E. Paul[3], J. Rautenberg, R. Renner, A. Stifutkin, J. Tandler, K.C. Voss, M. Wang, A. Weber[4]
Physikalisches Institut der Universität Bonn, Bonn, Germany [b]

D.S. Bailey[5], N.H. Brook[5], J.E. Cole, B. Foster, G.P. Heath, H.F. Heath, S. Robins, E. Rodrigues[6], J. Scott, R.J. Tapper, M. Wing
H.H. Wills Physics Laboratory, University of Bristol, Bristol, United Kingdom [m]

M. Capua, A. Mastroberardino, M. Schioppa, G. Susinno
Calabria University, Physics Department and INFN, Cosenza, Italy [e]

J.Y. Kim, Y.K. Kim, J.H. Lee, I.T. Lim, M.Y. Pac[7]
Chonnam National University, Kwangju, Korea [g]

A. Caldwell[8], M. Helbich, X. Liu, B. Mellado, Y. Ning, S. Paganis, Z. Ren, W.B. Schmidke, F. Sciulli
Nevis Laboratories, Columbia University, Irvington on Hudson, New York 10027 [o]

J. Chwastowski, A. Eskreys, J. Figiel, K. Olkiewicz, P. Stopa, L. Zawiejski
Institute of Nuclear Physics, Cracow, Poland [i]

L. Adamczyk, T. Bołd, I. Grabowska-Bołd, D. Kisielewska, A.M. Kowal, M. Kowal, T. Kowalski, M. Przybycień, L. Suszycki, D. Szuba, J. Szuba[9]
Faculty of Physics and Nuclear Techniques, University of Mining and Metallurgy, Cracow, Poland [p]

A. Kotański[10], W. Słomiński[11]
Department of Physics, Jagellonian University, Cracow, Poland

V. Adler, L.A.T. Bauerdick[12], U. Behrens, I. Bloch, K. Borras, V. Chiochia, D. Dannheim, G. Drews, J. Fourletova, U. Fricke, A. Geiser, F. Goebel[8], P. Göttlicher[13], O. Gutsche, T. Haas, W. Hain, G.F. Hartner, S. Hillert, B. Kahle, U. Kötz, H. Kowalski[14], G. Kramberger, H. Labes, D. Lelas, B. Löhr, R. Mankel, I.-A. Melzer-Pellmann, M. Moritz[15], C.N. Nguyen, D. Notz, M.C. Petrucci[16], A. Polini, A. Raval, U. Schneekloth, F. Selonke[3], U. Stoesslein, H. Wessoleck, G. Wolf, C. Youngman, W. Zeuner
Deutsches Elektronen-Synchrotron DESY, Hamburg, Germany

S. Schlenstedt
DESY Zeuthen, Zeuthen, Germany

G. Barbagli, E. Gallo, C. Genta, P. G. Pelfer
University and INFN, Florence, Italy [e]

A. Bamberger, A. Benen, N. Coppola
Fakultät für Physik der Universität Freiburg i.Br., Freiburg i.Br., Germany [b]

M. Bell, P.J. Bussey, A.T. Doyle, C. Glasman, J. Hamilton, S. Hanlon, S.W. Lee, A. Lupi, D.H. Saxon, I.O. Skillicorn
Department of Physics and Astronomy, University of Glasgow, Glasgow, United Kingdom [m]

I. Gialas
Department of Engineering in Management and Finance, Univ. of Aegean, Greece

B. Bodmann, T. Carli, U. Holm, K. Klimek, N. Krumnack, E. Lohrmann, M. Milite, H. Salehi, S. Stonjek[17], K. Wick, A. Ziegler, Ar. Ziegler
Hamburg University, Institute of Exp. Physics, Hamburg, Germany [b]

C. Collins-Tooth, C. Foudas, R. Gonçalo[6], K.R. Long, A.D. Tapper
Imperial College London, High Energy Nuclear Physics Group, London, United Kingdom [m]

P. Cloth, D. Filges
Forschungszentrum Jülich, Institut für Kernphysik, Jülich, Germany

K. Nagano, K. Tokushuku[18], S. Yamada, Y. Yamazaki
Institute of Particle and Nuclear Studies, KEK, Tsukuba, Japan [f]

A.N. Barakbaev, E.G. Boos, N.S. Pokrovskiy, B.O. Zhautykov
Institute of Physics and Technology of Ministry of Education and Science of Kazakhstan, Almaty, Kazakhstan

H. Lim, D. Son
Kyungpook National University, Taegu, Korea [g]

K. Piotrzkowski
Institut de Physique Nucléaire, Université Catholique de Louvain, Louvain-la-Neuve, Belgium

F. Barreiro, O. González, L. Labarga, J. del Peso, E. Tassi, J. Terrón, M. Vázquez
Departamento de Física Teórica, Universidad Autónoma de Madrid, Madrid, Spain [l]

M. Barbi, F. Corriveau, S. Gliga, J. Lainesse, S. Padhi, D.G. Stairs
Department of Physics, McGill University, Montréal, Québec, Canada H3A 2T8 [a]

T. Tsurugai
Meiji Gakuin University, Faculty of General Education, Yokohama, Japan [f]

A. Antonov, P. Danilov, B.A. Dolgoshein, D. Gladkov, V. Sosnovtsev, S. Suchkov
Moscow Engineering Physics Institute, Moscow, Russia [j]

R.K. Dementiev, P.F. Ermolov, Yu.A. Golubkov, I.I. Katkov, L.A. Khein, I.A. Korzhavina, V.A. Kuzmin, B.B. Levchenko[19], O.Yu. Lukina, A.S. Proskuryakov, L.M. Shcheglova, N.N. Vlasov, S.A. Zotkin
Moscow State University, Institute of Nuclear Physics, Moscow, Russia [k]

N. Coppola, S. Grijpink, E. Koffeman, P. Kooijman, E. Maddox, A. Pellegrino, S. Schagen, H. Tiecke, J.J. Velthuis, L. Wiggers, E. de Wolf
NIKHEF and University of Amsterdam, Amsterdam, Netherlands [h]

N. Brümmer, B. Bylsma, L.S. Durkin, T.Y. Ling
Physics Department, Ohio State University, Columbus, Ohio 43210 [n]

A.M. Cooper-Sarkar, A. Cottrell, R.C.E. Devenish, J. Ferrando, G. Grzelak, S. Patel, M.R. Sutton, R. Walczak
Department of Physics, University of Oxford, Oxford United Kingdom [m]

A. Bertolin, R. Brugnera, R. Carlin, F. Dal Corso, S. Dusini, A. Garfagnini, S. Limentani, A. Longhin, A. Parenti, M. Posocco, L. Stanco, M. Turcato
Dipartimento di Fisica dell' Università and INFN, Padova, Italy [e]

E.A. Heaphy, F. Metlica, B.Y. Oh, J.J. Whitmore[20]
Department of Physics, Pennsylvania State University, University Park, Pennsylvania 16802 [o]

Y. Iga
Polytechnic University, Sagamihara, Japan [f]

G. D'Agostini, G. Marini, A. Nigro
Dipartimento di Fisica, Università 'La Sapienza' and INFN, Rome, Italy [e]

C. Cormack[21], J.C. Hart, N.A. McCubbin
Rutherford Appleton Laboratory, Chilton, Didcot, Oxon, United Kingdom [m]

C. Heusch
University of California, Santa Cruz, California 95064 [n]

I.H. Park
Department of Physics, Ewha Womans University, Seoul, Korea

N. Pavel
Fachbereich Physik der Universität-Gesamthochschule Siegen, Germany

H. Abramowicz, A. Gabareen, S. Kananov, A. Kreisel, A. Levy
Raymond and Beverly Sackler Faculty of Exact Sciences, School of Physics, Tel-Aviv University, Tel-Aviv, Israel [d]

M. Kuze
Department of Physics, Tokyo Institute of Technology, Tokyo, Japan [f]

T. Abe, T. Fusayasu, S. Kagawa, T. Kohno, T. Tawara, T. Yamashita
Department of Physics, University of Tokyo, Tokyo, Japan [f]

R. Hamatsu, T. Hirose[3], M. Inuzuka, S. Kitamura[22], K. Matsuzawa, T. Nishimura
Tokyo Metropolitan University, Department of Physics, Tokyo, Japan [f]

M. Arneodo[23], M.I. Ferrero, V. Monaco, M. Ruspa, R. Sacchi, A. Solano
Università di Torino, Dipartimento di Fisica Sperimentale and INFN, Torino, Italy [e]

T. Koop, G.M. Levman, J.F. Martin, A. Mirea
Department of Physics, University of Toronto, Toronto, Ontario, Canada M5S 1A7 [a]

J.M. Butterworth, C. Gwenlan, R. Hall-Wilton, T.W. Jones, M.S. Lightwood, B.J. West
Physics and Astronomy Department, University College London, London, United Kingdom [m]

J. Ciborowski[24], R. Ciesielski[25], R.J. Nowak, J.M. Pawlak, J. Sztuk[26], T. Tymieniecka[27], A. Ukleja[27], J. Ukleja, A.F. Żarnecki
Warsaw University, Institute of Experimental Physics, Warsaw, Poland [q]

M. Adamus, P. Plucinski
Institute for Nuclear Studies, Warsaw, Poland [q]

Y. Eisenberg, L.K. Gladilin[28], D. Hochman, U. Karshon, M. Riveline
Department of Particle Physics, Weizmann Institute, Rehovot, Israel [c]

D. Kçira, S. Lammers, L. Li, D.D. Reeder, A.A. Savin, W.H. Smith
Department of Physics, University of Wisconsin, Madison, Wisconsin 53706 [n]

A. Deshpande, S. Dhawan, P.B. Straub
Department of Physics, Yale University, New Haven, Connecticut 06520-8121 [n]

S. Bhadra, C.D. Catterall, S. Fourletov, G. Hartner, S. Menary, M. Soares, J. Standage
Department of Physics, York University, Ontario, Canada M3J 1P3 [a]

[1] also affiliated with University College London
[2] on leave of absence at University of Erlangen-Nürnberg, Germany
[3] retired
[4] self-employed
[5] PPARC Advanced fellow
[6] supported by the Portuguese Foundation for Science and Technology (FCT)
[7] now at Dongshin University, Naju, Korea
[8] now at Max-Planck-Institut für Physik, München/Germany
[9] partly supported by the Israel Science Foundation and the Israel Ministry of Science
[10] supported by the Polish State Committee for Scientific Research, grant no. 2 P03B 09322
[11] member of Dept. of Computer Science
[12] now at Fermilab, Batavia/IL, USA
[13] now at DESY group FEB
[14] on leave of absence at Columbia Univ., Nevis Labs., N.Y./USA
[15] now at CERN
[16] now at INFN Perugia, Perugia, Italy
[17] now at Univ. of Oxford, Oxford/UK
[18] also at University of Tokyo
[19] partly supported by the Russian Foundation for Basic Research, grant 02-02-81023
[20] on leave of absence at The National Science Foundation, Arlington, VA/USA
[21] now at Univ. of London, Queen Mary College, London, UK
[22] present address: Tokyo Metropolitan University of Health Sciences, Tokyo 116-8551, Japan
[23] also at Università del Piemonte Orientale, Novara, Italy
[24] also at Łódź University, Poland
[25] supported by the Polish State Committee for Scientific Research, grant no. 2 P03B 07222
[26] Łódź University, Poland
[27] supported by German Federal Ministry for Education and Research (BMBF), POL 01/043
[28] on leave from MSU, partly supported by University of Wisconsin via the U.S.-Israel BSF

[a] supported by the Natural Sciences and Engineering Research Council of Canada (NSERC)

[b] supported by the German Federal Ministry for Education and Research (BMBF), under contract numbers HZ1GUA 2, HZ1GUB 0, HZ1PDA 5, HZ1VFA 5

[c] supported by the MINERVA Gesellschaft für Forschung GmbH, the Israel Science Foundation, the U.S.-Israel Binational Science Foundation and the Benozyio Center for High Energy Physics

[d] supported by the German-Israeli Foundation and the Israel Science Foundation

[e] supported by the Italian National Institute for Nuclear Physics (INFN)

[f] supported by the Japanese Ministry of Education, Culture, Sports, Science and Technology (MEXT) and its grants for Scientific Research

[g] supported by the Korean Ministry of Education and Korea Science and Engineering Foundation

[h] supported by the Netherlands Foundation for Research on Matter (FOM)

[i] supported by the Polish State Committee for Scientific Research, grant no. 620/E-77/SPUB-M/DESY/P-03/DZ 247/2000-2002

[j] partially supported by the German Federal Ministry for Education and Research (BMBF)

[k] supported by the Fund for Fundamental Research of Russian Ministry for Science and Education and by the German Federal Ministry for Education and Research (BMBF)

[l] supported by the Spanish Ministry of Education and Science through funds provided by CICYT

[m] supported by the Particle Physics and Astronomy Research Council, UK

[n] supported by the US Department of Energy

[o] supported by the US National Science Foundation

[p] supported by the Polish State Committee for Scientific Research, grant no. 112/E-356/SPUB-M/DESY/P-03/DZ 301/2000-2002, 2 P03B 13922

[q] supported by the Polish State Committee for Scientific Research, grant no. 115/E-343/SPUB-M/DESY/P-03/DZ 121/2001-2002, 2 P03B 07022

1 Introduction

In ep deep inelastic scattering (DIS) at HERA, final-state hadrons are dominantly produced by interactions between virtual photons and incoming protons. Diffractive interactions, characterized by a large rapidity gap in the distribution of the final-state hadrons, have been observed and extensively studied at HERA [1, 2, 3, 4, 5, 6, 7, 8, 9]. The measurements of the diffractive DIS cross sections [2, 3, 4, 5, 7] have been quantified in terms of a diffractive structure function, F_2^D, defined in analogy with the proton structure function, F_2. The diffractive parton densities, determined from these measurements, are dominated by gluons. The diffractive process at HERA has often been considered to proceed through the exchange of an object carrying the quantum numbers of the vacuum, called the Pomeron ($I\!P$). In the resolved-Pomeron model [10], the exchanged Pomeron acts as a source of partons, one of which interacts with the virtual photon. In an alternative view, the diffractive process at HERA can be described by the dissociation of the virtual photon into a $q\bar{q}$ or $q\bar{q}g$ state which interacts with the proton by the exchange of two gluons or, more generally, a gluon ladder with the quantum numbers of the vacuum [11, 12, 13].

Charm production in diffractive DIS, which has also been measured by the H1 and ZEUS collaborations [14, 15], allows quantitative tests of the models due to the sensitivity of charm production to gluon-initiated processes [16]. Calculations based on a gluon-dominated resolved Pomeron predict a large charm rate in diffractive DIS [17, 18]. In the two-gluon-exchange models, the rate from the $q\bar{q}g$ state is similar to that predicted by the resolved-Pomeron model, while the rate from the $q\bar{q}$ state is lower.

In this analysis, charm production, tagged using $D^{*\pm}$ mesons, is studied in diffractive interactions identified by the presence of a large rapidity gap between the proton at high rapidities and the centrally-produced hadronic system. The luminosity for the present measurement is about two times larger than in the previous ZEUS study [15]. The increase in luminosity and an improved rapidity acceptance in the proton direction allow a more detailed comparison with the model predictions in a wider kinematic range. The open-charm contribution to the diffractive proton structure function is measured for the first time.

2 Experimental set-up

The analysis was performed with data taken from 1998 to 2000, when HERA collided electrons or positrons[1] with energy $E_e = 27.5\,\text{GeV}$ with protons of energy $E_p = 920\,\text{GeV}$

[1] Hereafter, both e^+ and e^- are referred to as electrons, unless explicitly stated otherwise.

yielding a centre-of-mass energy of 318 GeV. The results are based on the sum of the e^-p and e^+p samples, corresponding to integrated luminosities of $16.4 \pm 0.3\,\mathrm{pb}^{-1}$ and $65.3 \pm 1.5\,\mathrm{pb}^{-1}$, respectively.

A detailed description of the ZEUS detector can be found elsewhere [19]. A brief outline of the components that are most relevant for this analysis is given below. Charged particles are tracked in the central tracking detector (CTD) [20], which operates in a magnetic field of 1.43 T provided by a thin superconducting solenoid. The CTD consists of 72 cylindrical drift chamber layers, organised in nine superlayers covering the polar-angle[2] region $15^\circ < \theta < 164^\circ$. The transverse-momentum resolution for full-length tracks is $\sigma(p_T)/p_T = 0.0058p_T \oplus 0.0065 \oplus 0.0014/p_T$, with p_T in GeV.

The high-resolution uranium–scintillator calorimeter (CAL) [21] consists of three parts: the forward (FCAL), the barrel (BCAL) and the rear (RCAL) calorimeters. Each part is subdivided transversely into towers and longitudinally into one electromagnetic section (EMC) and either one (in RCAL) or two (in BCAL and FCAL) hadronic sections (HAC). The smallest subdivision of the calorimeter is called a cell. The CAL energy resolutions, as measured under test-beam conditions, are $\sigma(E)/E = 0.18/\sqrt{E}$ for electrons and $\sigma(E)/E = 0.35/\sqrt{E}$ for hadrons, with E in GeV. The timing resolution of the CAL is better than 1 ns for energy deposits greater than 4.5 GeV.

In 1998-2000, the forward plug calorimeter (FPC) [22] was installed in the 20×20 cm^2 beam hole of the FCAL, with a small hole of radius 3.15 cm in the centre to accommodate the beam pipe. The FPC increased the forward calorimetric coverage by about 1 unit of pseudorapidity to $\eta \leq 5$. The FPC consisted of a lead–scintillator sandwich calorimeter divided longitudinally into electromagnetic and hadronic sections that were read out separately by wavelength-shifting fibers and photomultipliers. The energy resolution, as measured under test-beam conditions, was $\sigma(E)/E = 0.41/\sqrt{E} \oplus 0.062$ and $\sigma(E)/E = 0.65/\sqrt{E} \oplus 0.06$ for electrons and pions, respectively, with E in GeV.

The position of electrons scattered at a small angle with respect to the electron beam direction was measured using the small-angle rear tracking detector (SRTD) [23]. The luminosity was determined from the rate of the bremsstrahlung process $ep \to e\gamma p$, where the photon was measured with a lead–scintillator calorimeter [24] located at $Z = -107$ m.

[2] The ZEUS coordinate system is a right-handed Cartesian system, with the Z axis pointing in the proton beam direction, referred to as the "forward direction", and the X axis pointing left towards the centre of HERA. The coordinate origin is at the nominal interaction point. The pseudorapidity is defined as $\eta = -\ln\left(\tan\frac{\theta}{2}\right)$, where the polar angle, θ, is measured with respect to the proton beam direction.

3 Kinematics and reconstruction of variables

The four-momenta k, k' and P label the incoming electron, outgoing electron and the incoming proton, respectively, in DIS events:

$$e(k) + p(P) \to e(k') + \text{anything}.$$

To describe the kinematics of DIS events, any two of the following invariants can be used:

$$Q^2 = -q^2 = -(k - k')^2;\ x = \frac{Q^2}{2P \cdot q};\ y = \frac{P \cdot q}{P \cdot k};\ W^2 = \frac{Q^2(1-x)}{x},$$

where Q^2 is the negative square of the four-momentum q carried by the virtual photon, x is the Bjorken scaling variable, y is the fraction of the electron energy transferred to the proton in its rest frame, and W is the centre-of-mass energy of the photon-proton system. The scattered electron was identified using an algorithm based on a neural network [25]. The hadronic final state was reconstructed using combinations of CTD tracks and energy clusters measured in the CAL and FPC to form energy-flow objects (EFOs) [5,7,26]. The kinematic variables were reconstructed using the double-angle method [27].

To describe the diffractive process $ep \to eXp$, where X is the hadronic final state originating from the dissociation of the virtual photon, two additional variables were used:

- $x_{I\!P} = \frac{Q^2+M_X^2}{Q^2+W^2}$, where M_X is the invariant mass of the system X. This variable is the fraction of the incoming proton momentum carried by the diffractive exchange;
- $\beta = \frac{x}{x_{I\!P}} = \frac{Q^2}{Q^2+M_X^2}$. In an interpretation in which partonic structure is ascribed to the diffractive exchange, β is the longitudinal momentum fraction of the exchange that is carried by the struck quark.

The above expressions neglect the proton mass. The square of the four-momentum transfer at the proton vertex, t, was not measured; thus all results are implicitly integrated over this variable, which was assumed to be zero in the expressions for $x_{I\!P}$ and β.

The mass of the diffractive system X was calculated from EFOs using:

$$M_X^2 = \left(\sum_i E_i\right)^2 - \left(\sum_i P_{X,i}\right)^2 - \left(\sum_i P_{Y,i}\right)^2 - \left(\sum_i P_{Z,i}\right)^2,$$

where the sum i runs over the EFOs not associated with the scattered electron.

The process studied in this paper is $ep \to eXp \to e(D^{*\pm}X')p$, in which the system X includes at least one $D^{*\pm}$ meson. The latter was reconstructed using the mass-difference method [28] in the decay channel $D^{*+} \to D^0\pi_s^+$ followed by $D^0 \to K^-\pi^+(+c.c.)$, where

π_s indicates the "slow" pion. The fractional momentum of the $D^{*\pm}$ in the photon-proton system is defined as

$$x(D^{*\pm}) = \frac{2|p^*(D^{*\pm})|}{W},$$

where $p^*(D^{*\pm})$ is the $D^{*\pm}$ momentum in the photon-proton centre-of-mass frame.

4 Models of diffractive charm production

In the *resolved-Pomeron* model, proposed by Ingelman and Schlein [10], the exchanged Pomeron is assumed to be a object with a partonic structure. The diffractive cross section factorises into a Pomeron flux factor, describing the probability to find a Pomeron in the proton; the Pomeron's parton density function (PDF), specifying the probability to find a given parton in the Pomeron; and the interaction cross section with the parton. Within this model, open charm is produced in diffractive DIS via the boson-gluon-fusion (BGF) process, where the virtual photon interacts with a gluon from the Pomeron (Fig. 1a). The HERA measurements of the inclusive diffractive differential cross sections were found to be consistent with the resolved-Pomeron model with a Pomeron structure dominated by gluons. For $x_{I\!P} > 0.01$, an additional contribution from Reggeon exchanges, carrying the quantum numbers of a ρ, ω, a or f meson, was found to be sizeable [4]. A combined fit of the Pomeron parton densities to the H1 and ZEUS inclusive diffractive DIS measurements [4, 3, 29, 5] and to the ZEUS data on diffractive dijet photoproduction [30] has been made by Alvero et al. (ACTW) [31]. The Pomeron flux factor was assumed to be of the Donnachie-Landshoff form [32] and only data satisfying $x_{I\!P} < 0.01$ were used. To fit the Pomeron parton densities, five functional forms (labelled A, B, C, D and SG) were used. It was found that only gluon-dominated fits (B, D and SG) were able to describe both the DIS and photoproduction data, while the quark-dominated fits (A and C) underestimated the photoproduction data significantly. Therefore, only the gluon-dominated fits are compared to the data in Section 8. The fit results have been interfaced to the program HVQDIS [33] to calculate cross sections for diffractive charm production in DIS [18], both to leading and next-to-leading order (NLO) in QCD. In this analysis, the ACTW NLO predictions were calculated setting the charm-quark mass $m_c = 1.45\,\text{GeV}$ and the renormalisation and factorisation scales $\mu_R = \mu_F = \sqrt{Q^2 + 4m_c^2}$ as in [18]. The Peterson fragmentation function (with $\epsilon = 0.035$ [34]) was used for the charm decay. The probability for charm to fragment into a $D^{*\pm}$ meson was set to $f(c \to D^{*+}) = 0.235$ [35].

The *two-gluon-exchange* models consider fluctuations of the virtual photon into $q\bar{q}$ or $q\bar{q}g$ colour dipoles that interact with the proton via colour-singlet exchange; the simplest form of which is a pair of gluons [36]. The virtual-photon fluctuations into $c\bar{c}$ (Fig. 1b)

and $c\bar{c}g$ states (Fig. 1c) can lead to diffractive open-charm production. At high $x_{I\!P}$ values, quark exchanges are expected to become significant. Thus, the two-gluon-exchange calculations are expected to be valid only at low $x_{I\!P}$ values ($x_{I\!P} < 0.01$). In recent calculations [37, 12, 38, 39], the cross section for two-gluon exchange is related to the square of the unintegrated gluon distribution of the proton which depends on the gluon transverse momentum, k_T, relative to the proton direction. In the "saturation" model [39, 40], the calculation of the $q\bar{q}g$ cross section is performed under the assumption of strong k_T ordering of the final-state partons, which corresponds to $k_T^{(g)} \ll k_T^{(q,\bar{q})}$. The parameters of the model were tuned to describe the total photon-proton cross section measured at HERA. Alternatively, in the model of Bartels et al. [37, 12, 38], configurations without strong k_T ordering are included in the $q\bar{q}g$ cross-section calculation and the minimum value for the final-state-gluon transverse momentum, $k_{T,g}^{\rm cut}$, is a free parameter. The sum of the $c\bar{c}$ and $c\bar{c}g$ contributions in the saturation model and the model of Bartels et al. are hereafter referred to as SATRAP and BJLW, respectively. Both the SATRAP and BJLW predictions were calculated using the MC generator RAPGAP 2.08/06 [41], the proton PDF parameterisation GRV94HO [42], $m_c = 1.45\,\text{GeV}$ and $\mu_R = \mu_F = \sqrt{p_{c,T}^2 + 4m_c^2}$, where $p_{c,T}$ is the transverse momentum of the charm quark. Such scale form was used because RAPGAP does not provide the form used for the ACTW predictions. The probability for open charm to fragment into a $D^{*\pm}$ meson was set to $f(c \to D^{*+}) = 0.235$. In the BJLW calculation of the $c\bar{c}g$ component, the value of the parameter $k_{T,g}^{\rm cut}$ was set to 1.5 GeV [43].

5 Acceptance calculation

To study trigger and selection efficiencies, two MC programs, RAPGAP and RIDI 2.0 [44], were used to model the final states in the process $ep \to eXp \to e(D^{*\pm}X')p$.

The RAPGAP generator was used in the resolved-Pomeron mode, in which charm quarks are produced via the leading-order BGF process of Fig. 1a. The higher-order QCD corrections were simulated using the colour-dipole model implemented in ARIADNE 4.03 [45]. The LUND string model [46] as implemented in JETSET 7.4 [47] was used for hadronisation. The charm-quark mass was set to the default value of 1.5 GeV. The diffractive sample was generated assuming a gluon-dominated Pomeron, with a parameterisation from the H1 Collaboration called "H1 fit 2" [14]. The Reggeon (meson) component of the parameterisation was not used.

The RIDI generator is based on the two-gluon-exchange model developed by Ryskin [44]. To simulate the gluon momentum density, the GRV94HO proton PDF parameterisation was used. Final-state parton showers and hadronisation were simulated using JETSET and the charm-quark mass was set to the default value of 1.35 GeV. First-order radiative

corrections were included in the simulation although their effects were negligible. The $c\bar{c}$ and $c\bar{c}g$ components were generated separately and later combined in the proportion $16\% : 84\%$ which provided the best description of the β distribution of the data.

The RAPGAP MC sample was used to evaluate the acceptance. Three MC samples were used to estimate the model dependence of the acceptance corrections: the RIDI MC sample, a sample generated with RAPGAP using parton showers as implemented in LEPTO 6.1 [48] to simulate the higher-order QCD corrections, and a sample generated with RAPGAP using the Pomeron PDF parameterisation "H1 fit 3" [14].

To estimate the non-diffractive DIS background and to measure the ratio of diffractive to inclusive $D^{*\pm}$ production (see Section 8.2), two MC generators were used: RAPGAP in the non-diffractive mode for the nominal calculations and HERWIG 6.301 [49] as a systematic check. The RAPGAP parameters used were the same as those used in the ZEUS measurement of the inclusive DIS $D^{*\pm}$ cross sections [50]. To generate charm production via the leading-order BGF process with HERWIG, the CTEQ5L [51] proton PDF parameterisation and $m_c = 1.5\,\text{GeV}$ were used. Hadronisation in HERWIG is simulated with a cluster algorithm [52].

In this analysis, the final-state proton was not detected. To estimate and subtract the contribution from the diffractive processes where the proton dissociates into a system N, $ep \to eXN \to e(D^{*\pm}X')N$, four MC generators were used: DIFFVM [53] for the nominal calculations and RAPGAP, PHOJET [54] and EPSOFT 2.0 [55] for systematic checks. The DIFFVM MC program provides a detailed description of the proton-dissociative final state. The mass spectrum, M_N, of the system N is generated as a superposition of N^{*+} resonances and a continuum having the form $d\sigma/dM_N^2 \propto M_N^{-2(1+\epsilon)}$. The default parameter value $\epsilon = 0.0808$ [56] was used. In the RAPGAP simulation of proton dissociation, the proton splits into a quark and di-quark and the Pomeron is assumed to couple only to the single quark. The M_N spectrum follows a $1/M_N$ distribution. In PHOJET, M_N is calculated from the triple-Pomeron kinematics [54] and an approximation of the low-mass-resonance structure. In EPSOFT, the M_N-spectrum generation relies on a parameterisation of the $pp \to pN$ data.

The generated events were passed through the GEANT-based [57] simulation of the ZEUS detector and trigger. They were reconstructed by the same program chain as the data.

6 Event selection and $D^{*\pm}$ reconstruction

6.1 Trigger and DIS selection

Events were selected online with a three-level trigger [19, 58]. At the first level, events with an electron candidate in the EMC sections of RCAL or BCAL were selected [59]. In the latter case, a coincidence with a track originating at the nominal interaction point was required. At the second level, the non-ep background was further reduced by removing events with CAL timing inconsistent with an ep interaction. At the third level, events were fully reconstructed and selected by requiring a coincidence of a scattered-electron candidate found within the CAL and a $D^{*\pm}$ candidate reconstructed in the nominal decay mode using charged tracks measured by the CTD. The requirements were similar to, but looser than, the offline cuts described below. The efficiency of the online $D^{*\pm}$ reconstruction, determined relative to an inclusive DIS trigger, was above 95%.

The following criteria were applied offline to select DIS events:

- an electron with energy above 10 GeV;
- the impact point of the scattered electron on the RCAL lies outside the region 26×14 cm^2 centred on the beamline;
- $40 < \delta < 65$ GeV, where $\delta = \sum_i (E_i - P_{Z,i})$ and the sum runs over the EFOs from the hadronic system and the energy deposited by the identified electron;
- a vertex position $|Z_{\rm vtx}| < 50$ cm.

The events were restricted to the kinematic region $1.5 < Q^2 < 200\,\text{GeV}^2$ and $0.02 < y < 0.7$.

6.2 $D^{*\pm}$ reconstruction

Charged tracks with $p_T > 0.12\,\text{GeV}$ and $|\eta| < 1.75$ were selected. Only tracks assigned to the primary event vertex and with hits in at least three superlayers of the CTD were considered. Two oppositely charged tracks, each with $p_T > 0.5\,\text{GeV}$, were combined to form a D^0 candidate. The tracks were alternately assigned the mass of a charged kaon and a charged pion and the invariant mass of the track pair, $M(K\pi)$, was calculated. Only D^0 candidates that satisfy $1.81 < M(K\pi) < 1.92\,\text{GeV}$ were kept. Any additional track, with $p_T > 0.12\,\text{GeV}$ and charge opposite to that of the kaon track, was assigned the pion mass and combined with the D^0 candidate to form a $D^{*\pm}$ candidate with invariant mass $M(K\pi\pi_s)$. The $D^{*\pm}$ candidates were required to have $p_T(D^*) > 1.5\,\text{GeV}$ and $|\eta(D^*)| < 1.5$.

In the distribution of the mass difference, $\Delta M = M(K\pi\pi_s) - M(K\pi)$, for selected $D^{*\pm}$ candidates, a clear signal at the nominal value of $M(D^{*\pm}) - M(D^0)$ was observed (not shown). The combinatorial background under this signal was estimated from the mass-difference distribution for wrong-charge combinations, in which both tracks forming the D^0 candidates have the same charge and the third track has the opposite charge. The number of reconstructed $D^{*\pm}$ mesons was determined by subtracting the wrong-charge ΔM distribution after normalising it to the ΔM distribution of $D^{*\pm}$ candidates with the appropriate charges in the range $0.15 < \Delta M < 0.17\,\text{GeV}$. The subtraction, performed in the range $0.1435 < \Delta M < 0.1475\,\text{GeV}$, yielded an inclusive signal of 4976 ± 103 $D^{*\pm}$ mesons.

6.3 Selection of diffractive events

Diffractive events are characterised by the presence of a large rapidity gap between the proton at high rapidities and the centrally-produced hadronic system. To select such events, the following two requirements were applied:

- $E_{\text{FPC}} < 1.5\,\text{GeV}$, where E_{FPC} is the energy deposited in the FPC;
- $\eta_{\text{max}} < 3$, where η_{max} is the pseudorapidity of the most-forward EFO measured without using FPC information and with energy above 400 MeV.

This selection is illustrated in Fig. 2, where the distribution of η_{max} is shown for $D^{*\pm}$ mesons obtained after the wrong-charge-background subtraction. The data are compared to the η_{max} distributions of the non-diffractive RAPGAP and HERWIG MC samples and to the sum of the non-diffractive and diffractive RAPGAP MC. In Fig. 2a, the distributions are shown for events with any E_{FPC} value. The large peak at $\eta_{\text{max}} \sim 3.5$ corresponds to non-diffractive events in which the proton remnant deposits energy around the beam direction. On the low side of the peak, the contribution from non-diffractive interactions exhibits an exponential fall-off, leaving an excess at low values of η_{max} which is populated predominantly by diffractive events. Figure 2b shows that the requirement $E_{\text{FPC}} < 1.5\,\text{GeV}$ strongly suppresses the contribution from non-diffractive interactions. Requiring $\eta_{\text{max}} < 3$ in addition reduces the remaining non-diffractive background and ensures a gap of at least two units of pseudorapidity with respect to the edge of the forward calorimetric coverage (see Section 2).

The selected events were analysed in terms of the diffractive variables $x_{I\!P}$, β and M_X. To account for the restriction imposed by the $\eta_{\text{max}} < 3$ requirement, a cut of $x_{I\!P} < 0.035$ was applied. In addition, a cut of $\beta < 0.8$ was also used because diffractive charm production in DIS is strongly suppressed at large β values due the dominant contribution of events with small Q^2 and large M_X values.

Figure 3 shows the ΔM distribution after the above cuts. The number of $D^{*\pm}$ after the wrong-charge-background subtraction is 253 ± 21.

Figure 4 shows the number of reconstructed $D^{*\pm}$ mesons in bins of the variables $p_T(D^{*\pm})$, $\eta(D^{*\pm})$, $x(D^{*\pm})$, β, $x_{I\!P}$, $\log(M_X^2)$, $\log(Q^2)$ and W. The data are compared to the diffractive RAPGAP and RIDI simulations (normalised to the data). Both simulations reproduce the shapes of the data.

6.4 Subtraction of the proton-dissociative contribution

Diffractive events with proton dissociation can pass the $E_{\rm FPC} < 1.5\,{\rm GeV}$ and $\eta_{\rm max} < 3$ requirements if the major part of the proton-dissociative system escapes undetected down the forward beampipe. The proton-dissociative contribution was determined from the distribution of $E_{\rm FPC}$ for events selected with relaxed $D^{*\pm}$ reconstruction cuts and without cutting on $E_{\rm FPC}$. To ensure a gap of at least two units of pseudorapidity between the proton-dissociative system, tagged by the FPC, and the system X, a requirement of $\eta_{\rm max} < 1.75$ was applied. Figure 5 compares the $E_{\rm FPC}$ distribution for these events to the distributions of the diffractive RAPGAP and proton-dissociative DIFFVM MC samples. The MC samples were combined in the proportion providing the best description of the $E_{\rm FPC}$ distribution, and their sum was normalised to the data. Using the normalisation factors obtained for the two MC samples, the proton-dissociative contribution was calculated for the nominal diffractive selection described in Section 6.3. The proton-dissociative contribution was determined to be 16% with negligible statistical uncertainty; the systematic uncertainty was obtained as follows, where the effects of each source are shown in parentheses:

- the parameter b, regulating the shape of the M_N continuum distribution in the DIFFVM MC simulation, was varied between 0.7 and 1.5 ($^{+3.7}_{-3.0}\%$);
- uncertainties in the low-mass resonance structure and other details of the simulation of the proton-dissociative system were estimated by using the PHOJET, RAPGAP and EPSOFT MC generators ($^{+1.6}_{-0.9}\%$);
- a shift of $\pm 10\%$ due to the FPC energy-scale uncertainty ($^{+0.5}_{-0.1}\%$);
- a larger area, including the FPC and neighbouring FCAL towers, was used to tag the proton-dissociative system (-2.7%). This check is sensitive to the high-M_N proton-dissociative contribution and to details of the FPC and FCAL simulation.

These systematic uncertainties were added in quadrature separately for the positive and negative variations to determine the overall systematic uncertainty of $\pm 4.1\%$. The proton-dissociative contribution of $(16 \pm 4)\%$ was assumed to be independent of all kinematic variables and was subtracted from all measured cross sections.

7 Systematic uncertainties

The systematic uncertainties of the measured cross sections were determined by changing the selection cuts or the analysis procedure in turn and repeating the extraction of the cross sections [60]. The major sources of the systematic uncertainty were as the follows, where effects on the integrated cross section are shown in parentheses:

- the selection of inclusive DIS events ($^{+2.3}_{-3.3}\%$). Variations were made in the cut on the scattered-electron energy, the RCAL box cut, the δ cut and the vertex-position cut. In addition, both Q^2 and y were determined using the $e\Sigma$ method [61] rather than using the DA method;
- the selection of $D^{*\pm}$ candidates and background estimation ($^{+4.5}_{-3.7}\%$). The minimum transverse momentum for the K and π candidates was raised and lowered by 25 MeV. For the slow pion, π_s, the minimum transverse momentum was raised and lowered by 10 MeV. The signal region for $M(D^0)$ was loosened to $1.80 < M(D^0) < 1.93$ GeV and that of the ΔM distribution was widened to $0.143 < \Delta M < 0.148$ GeV. The ΔM background-normalisation region was varied by 5 MeV;
- the selection of diffractive events ($^{+3.9}_{-1.4}\%$). The requirements on $\eta_{\max}$ and E_{FPC} were varied by ± 0.2 units and ± 0.5 GeV, respectively;
- a shift of $\pm 3\%$ due to the CAL energy-scale uncertainty ($^{+0.7}_{-0.3}\%$);
- a shift of $\pm 10\%$ due to the FPC energy-scale uncertainty ($^{+0.2}_{-0.3}\%$);
- the model dependence of the non-diffractive contribution (-6.6%). This uncertainty was estimated using the HERWIG sample;
- the model dependence of the acceptance corrections ($^{+1.6}_{-7.4}\%$). This uncertainty was estimated using the RIDI MC sample, the RAPGAP sample generated with the LEPTO parton showers and the RAPGAP sample generated with the "H1 fit 3" parameterisation of the Pomeron structure function.

These systematic uncertainties were added in quadrature separately for the positive and negative variations to determine the overall systematic uncertainty of $^{+6.6}_{-11.2}\%$. These estimates were also made in each bin in which the differential cross sections were measured.

The normalisation uncertainties in the luminosity measurement ($\pm 2.2\%$) and the $D^{*\pm}$ and D^0 branching ratios ($\pm 2.5\%$ [62]) were not included in the systematic uncertainty. The uncertainty arising from the subtraction of the proton-dissociative background, quoted separately, is $\pm 4.1\%/0.84 = \pm 4.9\%$.

8 Results

8.1 Cross sections

The differential $D^{*\pm}$ cross sections for any given variable ξ were determined using:

$$\frac{d\sigma}{d\xi} = \frac{N(D^*)\ (1 - f_{pd})}{A\ \mathcal{L}\ B\ \Delta\xi},$$

where $N(D^*)$ is the number of $D^{*\pm}$ mesons in a bin of width $\Delta\xi$, A is the acceptance for that bin, $\mathcal{L}$ is the integrated luminosity, B is the product of the $D^{*+} \to D^0\pi_s^+$ and $D^0 \to K^-\pi^+$ branching ratios (0.0257 [62]), and f_{pd} (0.16) is the fraction of the proton-dissociative background discussed in Section 6.4.

Using the overall acceptance of 19.4%, the cross section for diffractive $D^{*\pm}$ production in the kinematic region $1.5 < Q^2 < 200\,\mathrm{GeV}^2$, $0.02 < y < 0.7$, $x_{I\!P} < 0.035$, $\beta < 0.8$, $p_T(D^{*\pm}) > 1.5\,\mathrm{GeV}$ and $|\eta(D^{*\pm})| < 1.5$ is

$$\sigma_{ep\to eD^{*\pm}X'p} = 521 \pm 43(\mathrm{stat.})^{+34}_{-58}(\mathrm{syst.}) \pm 26(\mathrm{p.diss.})\,\mathrm{pb},$$

where the last uncertainty arises from the subtraction of the proton-dissociative background[3].

In the case of Reggeon exchanges, open charm can be produced in the BGF process if the exchanged-meson PDF contains gluons. The Reggeon contribution to diffractive $D^{*\pm}$ production in the measured kinematic range was estimated to be less than 6% using RAPGAP with the Pomeron and meson PDF parameterisations "H1 fit 2" or "H1 fit 3". The contribution is less than 0.5% for $x_{I\!P} < 0.01$; it increases with $x_{I\!P}$, contributing about 12% in the last bin. The Reggeon contribution, which is smaller than the statistical uncertainty of the measurement, was neglected.

Figure 6 (Table 1) shows the differential cross section as a function of $x_{I\!P}$. The data are compared with the ACTW NLO predictions, calculated with the gluon-dominated fit B, the SATRAP predictions and the BJLW predictions. All three models agree with the data within experimental uncertainties below $x_{I\!P} = 0.01$. For larger $x_{I\!P}$ values, the ACTW and SATRAP models agree with the data whereas the BJLW prediction underestimates the measured cross sections as expected (see Section 4).

The differential cross sections as functions of $p_T(D^{*\pm})$, $\eta(D^{*\pm})$, $\log(M_X^2)$, $x(D^{*\pm})$, β, $\log(\beta)$, $\log(Q^2)$ and W were measured for $x_{I\!P} < 0.01$ and $x_{I\!P} < 0.035$ (Tables 2 and 3). Figure 7 compares the differential cross sections measured for $x_{I\!P} < 0.01$ with the ACTW,

[3] The diffractive $D^{*\pm}$ cross section was also calculated in the kinematic regions in which previous measurements [14, 15] were reported and was found to be consistent.

SATRAP and BJLW predictions. In Figs. 8 and 9, the ACTW and SATRAP predictions are compared with the differential cross sections measured for $x_{I\!P} < 0.035$.

The two-gluon-exchange BJLW model predictions, obtained with the cutoff value $k_{T,g}^{\rm cut} = 1.5\,\text{GeV}$ tuned using the H1 measurement [14], describe the differential cross sections in the range $x_{I\!P} < 0.01$ both in shape and normalisation. Using the value $k_{T,g}^{\rm cut} = 1.0\,\text{GeV}$ (2.0 GeV), the model predictions significantly overestimate (underestimate) the data in this range (not shown).

The two-gluon-exchange saturation model (SATRAP) predictions reproduce the shapes and the normalisations of the differential cross sections measured in both $x_{I\!P}$ ranges.

The ACTW NLO predictions, obtained with the gluon-dominated fit B, describe the data reasonably well in both $x_{I\!P}$ ranges. Using other gluon-dominated fits, the predictions significantly overestimate (fit D) or underestimate (fit SG) the data (not shown). The quark-dominated fits A and C were excluded by the previous ZEUS measurement [15].

8.2 Ratio of diffractive to inclusive $D^{*\pm}$ production

The ratio of diffractively produced $D^{*\pm}$ mesons to inclusive $D^{*\pm}$ mesons, R_D, was measured for $x < 0.028$. This limit is the product of the $x_{I\!P}$ and β requirements imposed for the diffractive $D^{*\pm}$ sample. The ratio of diffractive to inclusive DIS $D^{*\pm}$ production is then defined by

$$R_D = \frac{\sigma_{ep\to eD^{*\pm}X'p}(x_{I\!P} < 0.035, \beta < 0.8)}{\sigma_{ep\to eD^{*\pm}Y}(x < 0.028)}.$$

Sources of systematic uncertainty in the ratio measurement were studied in a similar manner to those for the cross-section measurements. There is a cancellation between the common systematic uncertainties originating from the selection of inclusive DIS events, the selection of $D^{*\pm}$ candidates and the background estimation. An additional contribution originates from the model dependence of the acceptance corrections used in the evaluation of the inclusive DIS $D^{*\pm}$ cross sections. This systematic uncertainty was estimated using the inclusive RAPGAP MC sample generated with LEPTO parton showers instead of the ARIADNE higher-order QCD corrections and with the HERWIG MC sample.

The ratio measured in the kinematic region $1.5 < Q^2 < 200\,\text{GeV}^2$, $0.02 < y < 0.7$, $p_T(D^{*\pm}) > 1.5\,\text{GeV}$, $|\eta(D^{*\pm})| < 1.5$ and $x < 0.028$ is

$$R_D = 6.4 \pm 0.5(\text{stat.})^{+0.3}_{-0.7}(\text{syst.})^{+0.3}_{-0.3}(\text{p.diss.})\ \%.$$

The value is consistent with previous measurements performed in similar kinematic ranges [14, 15].

Figure 10 (Table 4) shows the ratio measured as a function of $p_T(D^{*\pm})$, $\eta(D^{*\pm})$, $x(D^{*\pm})$, $\log(Q^2)$ and W. The measured R_D shows no dependence on Q^2, W or $x(D^{*\pm})$. The relative diffractive contribution is larger at small $p_T(D^{*\pm})$ and in the backward direction (negative $\eta(D^{*\pm})$). The NLO QCD predictions for the ratio of diffractive to inclusive DIS $D^{*\pm}$ production were obtained using ACTW NLO fit B for the diffractive predictions and the HVQDIS program with the CTEQ5F3 [51] proton PDF for the inclusive predictions. Parameters in both calculations were set to the values discussed in Section 4. The NLO QCD predictions reproduce the measured R_D values and the trends observed for the R_D distributions measured as functions of $p_T(D^{*\pm})$ and $\eta(D^{*\pm})$.

8.3 Open-charm contribution to the diffractive proton structure function $F_2^{D(3)}$

Neglecting contributions from Z-boson exchange and the longitudinal structure function, the open-charm contribution to the diffractive structure function of the proton can be related to the cross section, measured in the full $D^{*\pm}$ kinematic region, by

$$\frac{1}{2f(c\to D^{*+})}\frac{\mathrm{d}^3\sigma_{ep\to eD^{*\pm}X'p}}{\mathrm{d}x_{I\!P}\mathrm{d}\beta\mathrm{d}Q^2}=\frac{4\pi\alpha_{em}^2}{Q^4\beta}(1-y+\frac{y^2}{2})F_2^{D(3),c\bar{c}}(\beta,Q^2,x_{I\!P}). \qquad (1)$$

In order to estimate $F_2^{D(3),c\bar{c}}$, the differential cross section was measured as a function of $\log(\beta)$ for different regions of Q^2 and $x_{I\!P}$ (Table 5). Extrapolation factors of the measured cross sections to the full $p_T(D^{*\pm})$ and $\eta(D^{*\pm})$ phase space were estimated using the ACTW NLO fit B predictions. The factors were about five for low-$x_{I\!P}$ bins and two for high-$x_{I\!P}$ bins.

In each bin, $F_2^{D(3),c\bar{c}}$ was determined using the formula

$$F_{2\ \mathrm{meas}}^{D(3),c\bar{c}}(\beta_i,Q_i^2,x_{I\!P,i})=\frac{\sigma_{ep\to eD^{*\pm}X'p}^{i,\mathrm{meas}}}{\sigma_{ep\to eD^{*\pm}X'p}^{i,\mathrm{ACTW}}}F_{2\ \mathrm{ACTW}}^{D(3),c\bar{c}}(\beta_i,Q_i^2,x_{I\!P,i}),$$

where the cross sections σ^i in bin i are those for $p_T(D^{*\pm})>1.5\,\mathrm{GeV}$ and $|\eta(D^{*\pm})|<1.5$. The functional form of $F_{2\ \mathrm{ACTW}}^{D(3),c\bar{c}}$, calculated using Eq. (1), was used to quote the results for $F_2^{D(3),c\bar{c}}$ at convenient values of β_i, Q_i^2 and $x_{I\!P,i}$ close to the centre-of-gravity of the bin.

The measured $F_2^{D(3),c\bar{c}}$ values are listed in Table 6 with their experimental uncertainties. Using ACTW NLO fit D had no significant effect on the measured values. Other sources of extrapolation uncertainties are small compared to the experimental uncertainties [50].

Figure 11 shows the quantity $x_{I\!P}F_2^{D(3),c\bar{c}}$ as a function of $\log(\beta)$ for different Q^2 and $x_{I\!P}$ values. In all cases, $x_{I\!P}F_2^{D(3),c\bar{c}}$ rises as β decreases. The curves show the theoretical

$x_{I\!P} F_2^{D(3),c\bar{c}}$ obtained using the ACTW NLO calculations with fit B, D and SG. The fit B prediction generally agrees with the data. The fit D (SG) prediction overestimates (underestimates) the measured $x_{I\!P} F_2^{D(3),c\bar{c}}$ at low β.

9 Summary

Diffractive $D^{*\pm}$ production has been measured in the kinematic region $1.5 < Q^2 < 200\,\mathrm{GeV}^2$, $0.02 < y < 0.7$, $x_{I\!P} < 0.035$, $\beta < 0.8$, $p_T(D^{*\pm}) > 1.5\,\mathrm{GeV}$ and $|\eta(D^{*\pm})| < 1.5$. The cross section integrated over this kinematic region is $521 \pm 43(\mathrm{stat.})^{+34}_{-58}(\mathrm{syst.}) \pm 26(\mathrm{p.diss.})$ pb. Differential cross sections have been compared to the predictions of different diffractive models. The ACTW NLO predictions, based on parton densities of the Pomeron obtained from combined fits to the inclusive diffractive DIS and diffractive dijet photoproduction measurements at HERA, describe the results reasonably well in the whole $x_{I\!P}$ range if the gluon-dominated fit B is used. The predictions of the two-gluon-exchange saturation model also reproduce the shapes and normalisations of the differential cross sections in the whole $x_{I\!P}$ range. The predictions of the two-gluon-exchange BJLW model describe the cross sections measured for $x_{I\!P} < 0.01$, if a minimum value for the transverse momentum of the final-state gluon of $k_{T,g}^{\mathrm{cut}} = 1.5\,\mathrm{GeV}$ is used.

The ratio of diffractive $D^{*\pm}$ production to inclusive DIS $D^{*\pm}$ production has been measured to be $R_D = 6.4 \pm 0.5(\mathrm{stat.})^{+0.3}_{-0.7}(\mathrm{syst.})^{+0.3}_{-0.3}(\mathrm{p.diss.})$ %. The ratio R_D shows no dependence on W, Q^2 or $x(D^{*\pm})$. The relative contribution from diffraction is larger at small $p_T(D^{*\pm})$ and in the backward direction (negative $\eta(D^{*\pm})$). The NLO QCD predictions reproduce the measured R_D.

The open-charm contribution, $F_2^{D(3),c\bar{c}}$, to the diffractive proton structure function has been extracted. For all values of Q^2 and $x_{I\!P}$, $F_2^{D(3),c\bar{c}}$ rises as β decreases. The results have been compared with the theoretical $F_2^{D(3),c\bar{c}}$ obtained using the ACTW NLO calculations with the gluon-dominated fits B, D and SG. The data exclude the fits D and SG, and are consistent with fit B. This demonstrates that the data have a strong sensitivity to the diffractive parton densities, and that diffractive PDFs in NLO QCD are able to consistently describe both inclusive diffractive DIS and diffractive charm production in DIS.

10 Acknowledgments

We would like to thank the DESY Directorate for their strong support and encouragement. The remarkable achievements of the HERA machine group were vital for the successful

completion of this work and are greatly appreciated. The design, construction and installation of the ZEUS detector have been made possible by the ingenuity and effort of many people who are not listed as authors. We thank J. Bartels and H. Jung for informative discussions.

References

[1] ZEUS Collab., M. Derrick et al., Phys. Lett. **B 315**, 481 (1993).

[2] H1 Collab., T. Ahmed et al., Phys. Lett. **B 348**, 681 (1995).

[3] ZEUS Collab., M. Derrick et al., Z. Phys. **C 68**, 569 (1995).

[4] H1 Collab., C. Adloff et al., Z. Phys. **C 76**, 613 (1997).

[5] ZEUS Collab., J. Breitweg et al., Eur. Phys. J. **C 1**, 81 (1998).

[6] H1 Collab., C. Adloff et al., Phys. Lett. **B 428**, 206 (1998).

[7] ZEUS Collab., J. Breitweg et al., Eur. Phys. J. **C 6**, 43 (1999).

[8] ZEUS Collab., S. Chekanov et al., Phys. Lett. **B 516**, 273 (2001).

[9] ZEUS Collab., S. Chekanov et al., Phys. Rev. **D 65**, 052001 (2002).

[10] G. Ingelman and P.E. Schlein, Phys. Lett. **B 152**, 256 (1985).

[11] H. Lotter, Phys. Lett. **B 406**, 171 (1997).

[12] J. Bartels, H. Jung and M. Wüsthoff, Eur. Phys. J. **C 11**, 111 (1999).

[13] E.M. Levin et al., Z. Phys. **C 74**, 671 (1997).

[14] H1 Collab., C. Adloff et al., Phys. Lett. **B 520**, 191 (2001).

[15] ZEUS Collab., S. Chekanov et al., Phys. Lett. **B 545**, 244 (2002).

[16] M.F. McDermott and G. Briskin, *Proc. Workshop on Future Physics at HERA*, G. Ingelman, A. De Roeck and R. Klanner (eds.), Vol. 2, p. 691. Hamburg, Germany, DESY (1996).

[17] T. Gehrmann and W.J. Stirling, Z. Phys. **C 70**, 89 (1996).

[18] L. Alvero, J.C. Collins and J.J. Whitmore, Preprint hep-ph/9806340, 1998.

[19] ZEUS Collab., U. Holm (ed.), *The ZEUS Detector*. Status Report (unpublished), DESY (1993), available on `http://www-zeus.desy.de/bluebook/bluebook.html`.

[20] N. Harnew et al., Nucl. Instr. and Meth. **A 279**, 290 (1989);
B. Foster et al., Nucl. Phys. Proc. Suppl. **B 32**, 181 (1993);
B. Foster et al., Nucl. Instr. and Meth. **A 338**, 254 (1994).

[21] M. Derrick et al., Nucl. Instr. and Meth. **A 309**, 77 (1991);
A. Andresen et al., Nucl. Instr. and Meth. **A 309**, 101 (1991);
A. Caldwell et al., Nucl. Instr. and Meth. **A 321**, 356 (1992);
A. Bernstein et al., Nucl. Instr. and Meth. **A 336**, 23 (1993).

[22] A. Bamberger et al., Nucl. Instr. and Meth. **A 450**, 235 (2000).

[23] A. Bamberger et al., Nucl. Instr. and Meth. **A 401**, 63 (1997).

[24] J. Andruszków et al., Preprint DESY-92-066, DESY, 1992;
ZEUS Collab., M. Derrick et al., Z. Phys. **C 63**, 391 (1994);
J. Andruszków et al., Acta Phys. Pol. **B 32**, 2025 (2001).

[25] H. Abramowicz, A. Caldwell and R. Sinkus, Nucl. Instr. and Meth. **A 365**, 508 (1995);
R. Sinkus and T. Voss, Nucl. Instr. and Meth. **A 391**, 360 (1997).

[26] G.M. Briskin, *Diffractive Dissociation in ep Deep Inelastic Scattering*. Ph.D. Thesis, Tel Aviv University, 1998. (Unpublished).

[27] S. Bentvelsen, J. Engelen and P. Kooijman, *Proc. Workshop on Physics at HERA*, W. Buchmüller and G. Ingelman (eds.), Vol. 1, p. 23. Hamburg, Germany, DESY (1992);
K.C. Höger, *Proc. Workshop on Physics at HERA*, W. Buchmüller and G. Ingelman (eds.), Vol. 1, p. 43. Hamburg, Germany, DESY (1992).

[28] S. Nussinov, Phys. Rev. Lett. **35**, 1672 (1975).

[29] ZEUS Collab., M. Derrick et al., Z. Phys. **C 70**, 391 (1996).

[30] ZEUS Collab., M. Derrick et al., Phys. Lett. **B 356**, 129 (1995).

[31] L. Alvero et al., Phys. Rev. **D 59**, 074022 (1999).

[32] A. Donnachie and P.V. Landshoff, Phys. Lett. **B 191** (1987);
A. Donnachie and P.V. Landshoff, Nucl. Phys. **B 303**, 634 (1988).

[33] B.W. Harris and J. Smith, Phys. Rev. **D 57**, 2806 (1998).

[34] C. Peterson et al., Phys. Rev. **D 27**, 105 (1983).

[35] L. Gladilin, Preprint hep-ex/9912064, 1999.

[36] F.E. Low, Phys. Rev. **D 12**, 163 (1975);
S. Nussinov, Phys. Rev. Lett. **34**, 1286 (1975);
S. Nussinov, Phys. Rev. **D 14**, 246 (1976).

[37] J. Bartels, H. Lotter and M. Wüsthoff, Phys. Lett. **B 379**, 239 (1996).

[38] J. Bartels, H. Jung and A. Kyrieleis, Eur. Phys. J. **C 24**, 555 (2002).

[39] K. Golec-Biernat and M. Wüsthoff, Phys. Rev. **D 59**, 014017 (1999).

[40] H. Kowalski, *Proc. Workshop on New Trends in HERA Physics*, G. Grindhammer, B.A. Kniehl and G. Kramer (eds.), pp. 361–380. (1999), available on `http://www-library.desy.de/conf/ringberg99.html`;
H. Kowalski and M. Wüsthoff, *Proc. 8th International Workshop Deep Inelastic*

Scattering and QCD, J. Gracey and T. Greenshaw (eds.), p. 192. World Scientific, Singapore (2000).

[41] H. Jung, Comp. Phys. Comm. **86**, 147 (1995).

[42] M. Glück, E. Reya and A. Vogt, Z. Phys. **C 67**, 433 (1995).

[43] J. Bartels, H. Jung and A. Kyrieleis, Preprint DESY-01-116 (hep-ph/0204269), 2002.

[44] M.G. Ryskin, Sov. J. Nucl. Phys. **52**, 529 (1990);
M.G. Ryskin and A. Solano, *Proc. Workshop on Monte Carlo Generators for HERA Physics*, G. Grindhammer, G. Ingelman, H. Jung and T. Doyle (eds.), p. 386. DESY, Hamburg, Germany (1999). Also in preprint DESY-PROC-1999-02, available on `http://www.desy.de/~heramc/`.

[45] L. Lönnblad, Comp. Phys. Comm. **71**, 15 (1992).

[46] B. Andersson et al., Phys. Rep. **97**, 31 (1983).

[47] T. Sjöstrand, Comp. Phys. Comm. **82**, 74 (1994).

[48] G. Ingelman, A. Edin and J. Rathsman, Comp. Phys. Comm. **101**, 108 (1997).

[49] G. Marchesini et al., Comp. Phys. Comm. **67**, 465 (1992).

[50] ZEUS Collab., J. Breitweg et al., Eur. Phys. J. **C 12**, 35 (2000).

[51] CTEQ Collab., H.L. Lai et al., Eur. Phys. J. **C 12**, 375 (2000).

[52] B.R. Webber, Nucl. Phys. **B 238**, 492 (1984).

[53] B. List and A. Mastroberardino, *Proc. Workshop on Monte Carlo Generators for HERA Physics*, p. 396. DESY, Hamburg, Germany (1999). Also in preprint DESY-PROC-1999-02, available on `http://www.desy.de/~heramc/`.

[54] R. Engel, Z. Phys. **C 66**, 203 (1995);
R. Engel and J. Ranft, Phys. Rev. **D 54**, 4246 (1996).

[55] M. Kasprzak, *Inclusive Properties of Diffractive and Non-diffractive Photoproduction at HERA*. Ph.D. Thesis, Warsaw University, Warsaw, Poland, Report DESY F35D-96-16, DESY, 1996.

[56] A. Donnachie and P.V. Landshoff, Phys. Lett. **B 296**, 227 (1992).

[57] R. Brun et al., GEANT3, Technical Report CERN-DD/EE/84-1, CERN, 1987.

[58] W.H. Smith, K. Tokushuku and L.W. Wiggers, *Proc. Computing in High-Energy Physics (CHEP), Annecy, France, Sept. 1992*, C. Verkerk and W. Wojcik (eds.), p. 222. CERN, Geneva, Switzerland (1992). Also in preprint DESY 92-150B.

[59] W.H. Smith et al., Nucl. Instr. and Meth. **A 355**, 278 (1995).

[60] N.N. Vlasov, *Study of diffractive production of D^* mesons in reactions of deep inelastic ep scattering at HERA collider*. Ph.D. Thesis, Moscow State University, 2003. Unpublished.

[61] U. Bassler and G. Bernardi, Nucl. Instr. and Meth. **A 426**, 583 (1999).

[62] Particle Data Group, K. Hagiwara et al., Phys. Rev. **D 66**, 10001 (2002).

$x_{I\!P}$ bin	$\mathrm{d}\sigma/\mathrm{d}x_{I\!P}$ (nb)
0 , 0.003	$28.0 \pm 4.9^{+3.4}_{-3.2}$
0.003 , 0.006	$25.4 \pm 4.7^{+5.1}_{-2.4}$
0.006 , 0.010	$18.6 \pm 3.6^{+1.9}_{-2.5}$
0.010 , 0.020	$13.7 \pm 2.2^{+1.6}_{-2.3}$
0.020 , 0.035	$13.7 \pm 2.4^{+5.0}_{-2.9}$

Table 1: *Differential cross section for diffractive $D^{*\pm}$ production as a function of $x_{I\!P}$. The first and second uncertainties represent statistical and systematic uncertainties, respectively. The overall normalisation uncertainties arising from the luminosity measurement ($\pm 2.2\%$), from the $D^{*\pm}$ and D^0 branching ratios ($\pm 2.5\%$) and from the proton-dissociative background subtraction ($\pm 4.9\%$) are not indicated.*

$p_T(D^{*\pm})$ bin (GeV)	$\mathrm{d}\sigma/\mathrm{d}p_T(D^{*\pm})$ (pb/ GeV)	
	$x_{I\!P} < 0.01$	$x_{I\!P} < 0.035$
1.5 , 2.4	$161 \pm 29^{+28}_{-19}$	$307 \pm 50^{+44}_{-42}$
2.4 , 3.3	$66 \pm 11^{+8}_{-7}$	$151 \pm 20^{+16}_{-19}$
3.3 , 4.2	$19 \pm 5^{+2}_{-2}$	$70 \pm 11^{+4}_{-7}$
4.2 , 5.4	$10 \pm 3^{+1}_{-1}$	$26 \pm 5^{+3}_{-2}$
5.4 , 10.0		$2.8 \pm 0.9^{+0.3}_{-0.5}$
$\eta(D^{*\pm})$ bin	$\mathrm{d}\sigma/\mathrm{d}\eta(D^{*\pm})$ (pb)	
	$x_{I\!P} < 0.01$	$x_{I\!P} < 0.035$
-1.5 , -0.9	$124 \pm 26^{+13}_{-16}$	$212 \pm 36^{+27}_{-27}$
-0.9 , -0.3	$104 \pm 19^{+14}_{-6}$	$213 \pm 31^{+28}_{-30}$
-0.3 , 0.3	$78 \pm 17^{+11}_{-9}$	$195 \pm 29^{+32}_{-27}$
0.3 , 0.9	$37 \pm 13^{+8}_{-12}$	$125 \pm 28^{+18}_{-29}$
0.9 , 1.5	$55 \pm 20^{+21}_{-11}$	$134 \pm 36^{+38}_{-38}$
$\log(M_X^2/\,\mathrm{GeV}^2)$ bin	$\mathrm{d}\sigma/\mathrm{d}\log(M_X^2/\,\mathrm{GeV}^2)$ (pb)	
	$x_{I\!P} < 0.01$	$x_{I\!P} < 0.035$
1.00 , 1.44	$89 \pm 21^{+21}_{-17}$	$94 \pm 23^{+22}_{-21}$
1.44 , 1.88	$195 \pm 35^{+26}_{-25}$	$201 \pm 38^{+22}_{-28}$
1.88 , 2.32	$200 \pm 29^{+24}_{-21}$	$382 \pm 45^{+37}_{-46}$
2.32 , 2.76	$47 \pm 25^{+17}_{-16}$	$284 \pm 54^{+41}_{-60}$
2.76 , 3.20		$286 \pm 65^{+129}_{-102}$
$x(D^{*\pm})$ bin	$\mathrm{d}\sigma/\mathrm{d}x(D^{*\pm})$ (pb)	
	$x_{I\!P} < 0.01$	$x_{I\!P} < 0.035$
0.00 , 0.16	$185 \pm 61^{+62}_{-43}$	$429 \pm 107^{+161}_{-125}$
0.16 , 0.32	$252 \pm 76^{+74}_{-52}$	$788 \pm 135^{+163}_{-156}$
0.32 , 0.48	$446 \pm 85^{+39}_{-46}$	$864 \pm 134^{+76}_{-121}$
0.48 , 0.64	$376 \pm 75^{+67}_{-78}$	$726 \pm 119^{+106}_{-157}$
0.64 , 1.00	$92 \pm 21^{+18}_{-9}$	$221 \pm 38^{+27}_{-39}$

Table 2: *Differential cross sections for diffractive $D^{*\pm}$ production as a function of $p_T(D^{*\pm})$, $\eta(D^{*\pm})$, $\log(M_X^2)$ and $x(D^{*\pm})$. The first and second uncertainties are statistical and systematic, respectively. The overall normalisation uncertainties arising from the luminosity measurement ($\pm 2.2\%$), from the $D^{*\pm}$ and D^0 branching ratios ($\pm 2.5\%$) and from the proton-dissociative background subtraction ($\pm 4.9\%$) are not indicated.*

β bin	$\mathrm{d}\sigma/\mathrm{d}\beta$ (pb)	
	$x_{I\!P} < 0.01$	$x_{I\!P} < 0.035$
0.00 , 0.10	$1252 \pm 203^{+170}_{-118}$	$4153 \pm 410^{+243}_{-558}$
0.10 , 0.20	$419 \pm 94^{+32}_{-56}$	$654 \pm 125^{+125}_{-113}$
0.20 , 0.30	$244 \pm 54^{+40}_{-20}$	$311 \pm 69^{+62}_{-38}$
0.30 , 0.45	$100 \pm 35^{+15}_{-27}$	$91 \pm 39^{+22}_{-34}$
0.45 , 0.80	$27 \pm 11^{+14}_{-5}$	$33 \pm 13^{+15}_{-8}$
$\log(\beta)$ bin	$\mathrm{d}\sigma/\mathrm{d}\log(\beta)$ (nb)	
	$x_{I\!P} < 0.01$	$x_{I\!P} < 0.035$
-3.0 , -2.0		$115 \pm 33^{+58}_{-63}$
-2.0 , -1.5	$105 \pm 28^{+22}_{-33}$	$392 \pm 58^{+39}_{-74}$
-1.5 , -1.0	$124 \pm 25^{+27}_{-17}$	$272 \pm 41^{+40}_{-37}$
-1.0 , -0.5	$141 \pm 22^{+12}_{-13}$	$203 \pm 28^{+26}_{-26}$
-0.5 , -0.1	$65 \pm 16^{+14}_{-11}$	$56 \pm 18^{+17}_{-9}$
$\log(Q^2/\,\mathrm{GeV}^2)$ bin	$\mathrm{d}\sigma/\mathrm{d}\log(Q^2/\,\mathrm{GeV}^2)$ (pb)	
	$x_{I\!P} < 0.01$	$x_{I\!P} < 0.035$
0.17, 0.6	$276 \pm 51^{+51}_{-34}$	$534 \pm 87^{+46}_{-96}$
0.6 , 1.0	$140 \pm 29^{+26}_{-15}$	$324 \pm 51^{+35}_{-55}$
1.0 , 1.3	$106 \pm 27^{+8}_{-6}$	$342 \pm 50^{+28}_{-34}$
1.3 , 1.55	$103 \pm 25^{+10}_{-10}$	$225 \pm 43^{+13}_{-29}$
1.55 , 2.3	$17 \pm 7^{+4}_{-3}$	$41 \pm 13^{+16}_{-6}$
W bin (GeV)	$\mathrm{d}\sigma/\mathrm{d}W$ (pb/ GeV)	
	$x_{I\!P} < 0.01$	$x_{I\!P} < 0.035$
50 , 92	$0.45 \pm 0.14^{+0.13}_{-0.09}$	$1.53 \pm 0.35^{+0.23}_{-0.33}$
92 , 134	$1.48 \pm 0.29^{+0.23}_{-0.21}$	$3.36 \pm 0.49^{+0.45}_{-0.51}$
134 , 176	$1.63 \pm 0.29^{+0.16}_{-0.21}$	$3.68 \pm 0.49^{+0.32}_{-0.50}$
176 , 218	$1.25 \pm 0.29^{+0.25}_{-0.12}$	$2.43 \pm 0.44^{+0.41}_{-0.37}$
218 , 260	$0.50 \pm 0.33^{+0.22}_{-0.15}$	$0.95 \pm 0.48^{+0.48}_{-0.18}$

Table 3: *Differential cross sections for diffractive $D^{*\pm}$ production as a function of β, $\log(\beta)$, $\log(Q^2)$ and W. The first and second uncertainties are statistical and systematic, respectively. The overall normalisation uncertainties arising from the luminosity measurement ($\pm 2.2\%$), from the $D^{*\pm}$ and D^0 branching ratios ($\pm 2.5\%$) and from the proton-dissociative background subtraction ($\pm 4.9\%$) are not indicated.*

$p_T(D^{*\pm})$ bin (GeV)	R_D (%)
1.5 , 2.4	$8.5 \pm 1.5^{+0.9}_{-0.9}$
2.4 , 3.3	$6.3 \pm 0.9^{+0.2}_{-0.7}$
3.3 , 4.2	$5.5 \pm 0.9^{+0.3}_{-0.5}$
4.2 , 5.4	$4.3 \pm 0.9^{+0.4}_{-0.2}$
5.4 , 10.0	$2.5 \pm 0.8^{+0.2}_{-0.4}$
$\eta(D^{*\pm})$ bin	R_D (%)
-1.5 , -0.9	$11.2 \pm 2.0^{+0.9}_{-0.9}$
-0.9 , -0.3	$8.6 \pm 1.3^{+0.7}_{-1.1}$
-0.3 , 0.3	$6.8 \pm 1.1^{+0.5}_{-0.7}$
0.3 , 0.9	$4.4 \pm 1.0^{+0.5}_{-0.4}$
0.9 , 1.5	$4.4 \pm 1.2^{+0.9}_{-1.1}$
$x(D^{*\pm})$ bin	R_D (%)
0.00 , 0.16	$5.0 \pm 1.3^{+2.7}_{-1.1}$
0.16 , 0.32	$6.2 \pm 1.1^{+1.3}_{-1.0}$
0.32 , 0.48	$6.4 \pm 1.0^{+0.4}_{-0.7}$
0.48 , 0.64	$7.4 \pm 1.2^{+0.9}_{-1.6}$
0.64 , 1.00	$9.6 \pm 1.7^{+0.9}_{-2.5}$
$\log(Q^2/\,\mathrm{GeV}^2)$ bin	R_D (%)
0.17 , 0.60	$7.9 \pm 1.3^{+0.7}_{-0.7}$
0.60 , 1.00	$5.8 \pm 0.9^{+0.5}_{-1.0}$
1.00 , 1.30	$8.1 \pm 1.2^{+0.4}_{-0.7}$
1.30 , 1.55	$7.8 \pm 1.6^{+0.2}_{-0.7}$
1.55 , 2.30	$3.6 \pm 1.2^{+0.4}_{-0.4}$
W bin (GeV)	R_D (%)
50 , 92	$5.1 \pm 1.2^{+0.3}_{-1.2}$
92 , 134	$6.6 \pm 1.0^{+0.4}_{-1.0}$
134 , 176	$7.7 \pm 1.1^{+0.6}_{-0.8}$
176 , 218	$7.4 \pm 1.4^{+1.4}_{-0.7}$
218 , 260	$4.4 \pm 2.3^{+1.0}_{-0.8}$

Table 4: *Ratio of diffractively produced $D^{*\pm}$ mesons to inclusive $D^{*\pm}$ meson production as a function of $p_T(D^{*\pm})$, $\eta(D^{*\pm})$, $x(D^{*\pm})$, $\log(Q^2)$ and W. The first and second uncertainties are statistical and systematic, respectively. The overall normalisation uncertainties arising from the luminosity measurement ($\pm 2.2\%$), from the $D^{*\pm}$ and D^0 branching ratios ($\pm 2.5\%$) and from the proton-dissociative background subtraction ($\pm 4.9\%$) are not indicated.*

$\log(\beta)$ bin	$\mathrm{d}\sigma/\mathrm{d}\log(\beta)$, $x_{I\!P} < 0.01$ (pb)	
	$1.5 < Q^2 < 10$ GeV^2	$10 < Q^2 < 200$ GeV^2
-2.0 , -1.5	$107 \pm 28^{+23}_{-36}$	
-1.5 , -1.0	$114 \pm 25^{+30}_{-16}$	
-1.0 , -0.5	$62 \pm 16^{+14}_{-8}$	$80 \pm 15^{+6}_{-9}$
-0.5 , -0.1		$61 \pm 16^{+13}_{-9}$
$\log(\beta)$ bin	$\mathrm{d}\sigma/\mathrm{d}\log(\beta)$, $0.01 < x_{I\!P} < 0.035$ (pb)	
	$1.5 < Q^2 < 10$ GeV^2	$10 < Q^2 < 200$ GeV^2
-3.0 , -2.0	$96 \pm 31^{+53}_{-37}$	
-2.0 , -1.5	$142 \pm 43^{+36}_{-73}$	$141 \pm 30^{+44}_{-32}$
-1.5 , -1.0		$106 \pm 25^{+13}_{-20}$
-1.0 , -0.5		$52 \pm 17^{+22}_{-14}$

Table 5: *Differential cross section for diffractive $D^{*\pm}$ production as a function of $\log(\beta)$ for different regions of Q^2 and $x_{I\!P}$. The first and second uncertainties are statistical and systematic, respectively. The overall normalisation uncertainties arising from the luminosity measurement ($\pm 2.2\%$), from the $D^{*\pm}$ and D^0 branching ratios ($\pm 2.5\%$) and from the proton-dissociative background subtraction ($\pm 4.9\%$) are not indicated.*

$F_2^{D(3)c\bar{c}}$, $x_{I\!P} = 0.004$		
β	$Q^2 = 4\,\mathrm{GeV}^2$	$Q^2 = 25\,\mathrm{GeV}^2$
0.020	$1.34 \pm 0.35^{+0.28}_{-0.44}$	
0.050	$0.92 \pm 0.20^{+0.24}_{-0.13}$	
0.200	$0.20 \pm 0.05^{+0.05}_{-0.03}$	$2.14 \pm 0.40^{+0.16}_{-0.23}$
0.500		$0.89 \pm 0.23^{+0.18}_{-0.12}$
$F_2^{D(3)c\bar{c}}$, $x_{I\!P} = 0.02$		
β	$Q^2 = 4\,\mathrm{GeV}^2$	$Q^2 = 25\,\mathrm{GeV}^2$
0.005	$0.20 \pm 0.07^{+0.12}_{-0.08}$	
0.020	$0.17 \pm 0.05^{+0.04}_{-0.09}$	$1.87 \pm 0.40^{+0.59}_{-0.44}$
0.050		$0.50 \pm 0.12^{+0.06}_{-0.09}$
0.200		$0.18 \pm 0.06^{+0.08}_{-0.05}$

Table 6: *The measured charm contribution to the diffractive structure function of the proton, $F_2^{D(3),c\bar{c}}$, for different values of β, Q^2 and $x_{I\!P}$. The first and second uncertainties are statistical and systematic, respectively. The overall normalisation uncertainties arising from the luminosity measurement ($\pm 2.2\%$), from the $D^{*\pm}$ and D^0 branching ratios ($\pm 2.5\%$) and from the proton-dissociative background subtraction ($\pm 4.9\%$) are not indicated.*

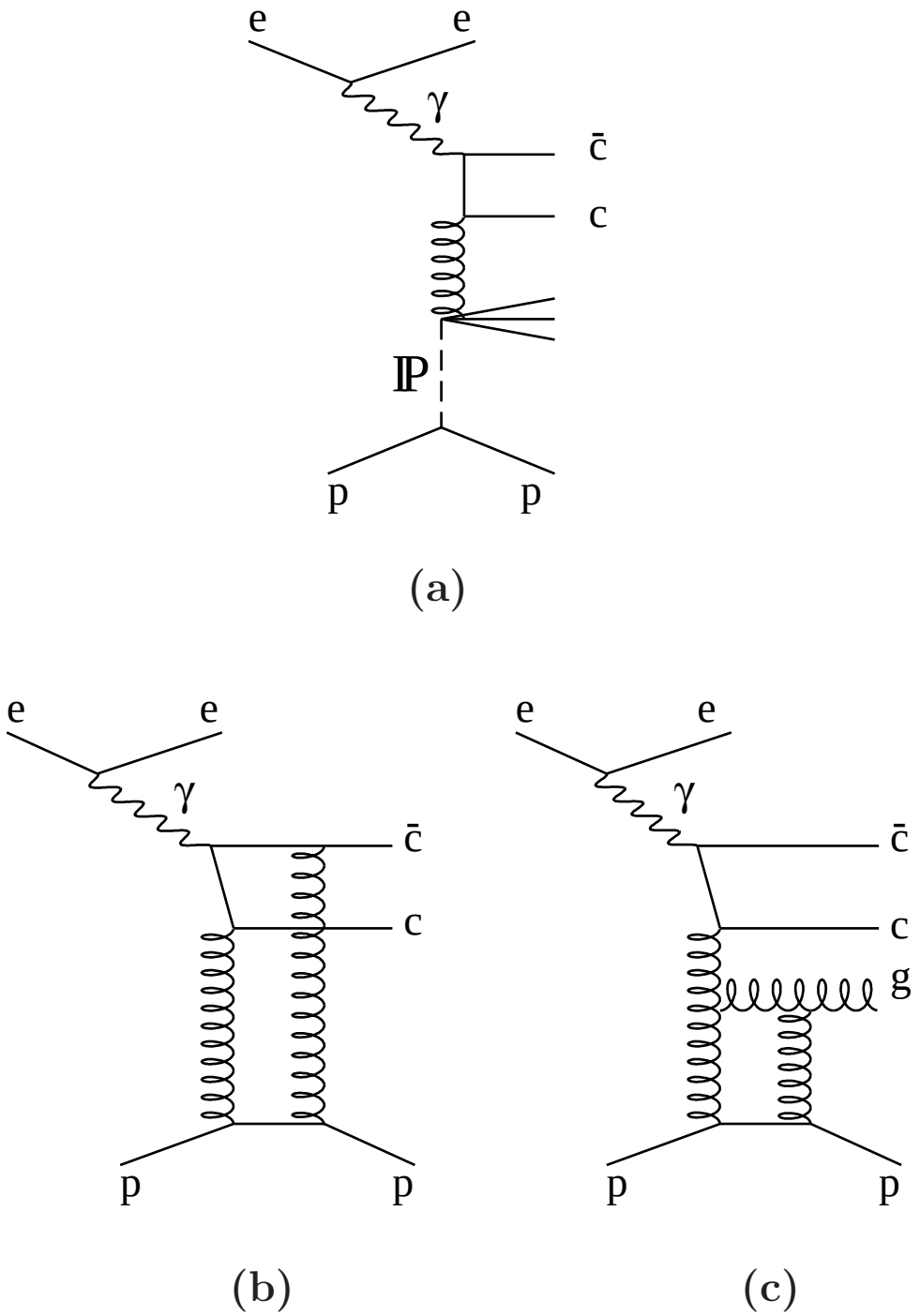

Figure 1: *Modelling charm production in diffractive ep scattering: (a) boson-gluon fusion in the resolved-Pomeron model, (b) $c\bar{c}$ and (c) $c\bar{c}g$ states in the two-gluon-exchange model.*

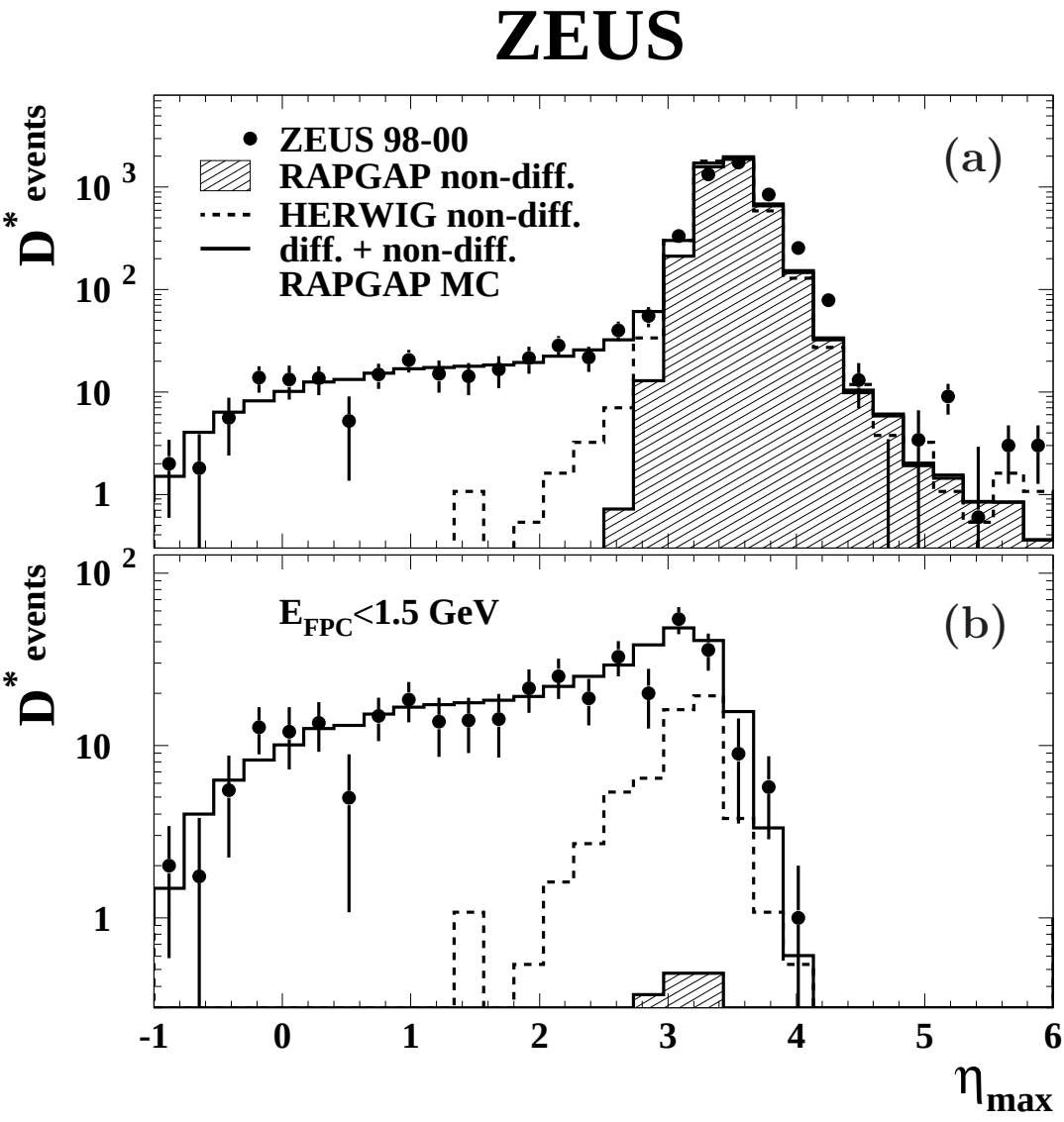

Figure 2: *Numbers of reconstructed $D^{*\pm}$ mesons (dots) as a function of $\eta_{\max}$ for DIS events with (a) any $E_{\rm FPC}$ values and (b) $E_{\rm FPC} < 1.5\,GeV$. The solid histogram shows the sum of the non-diffractive RAPGAP MC (hatched area) and the diffractive RAPGAP MC. The sum was normalised to have the same area as the data. The dashed histogram shows the non-diffractive HERWIG MC.*

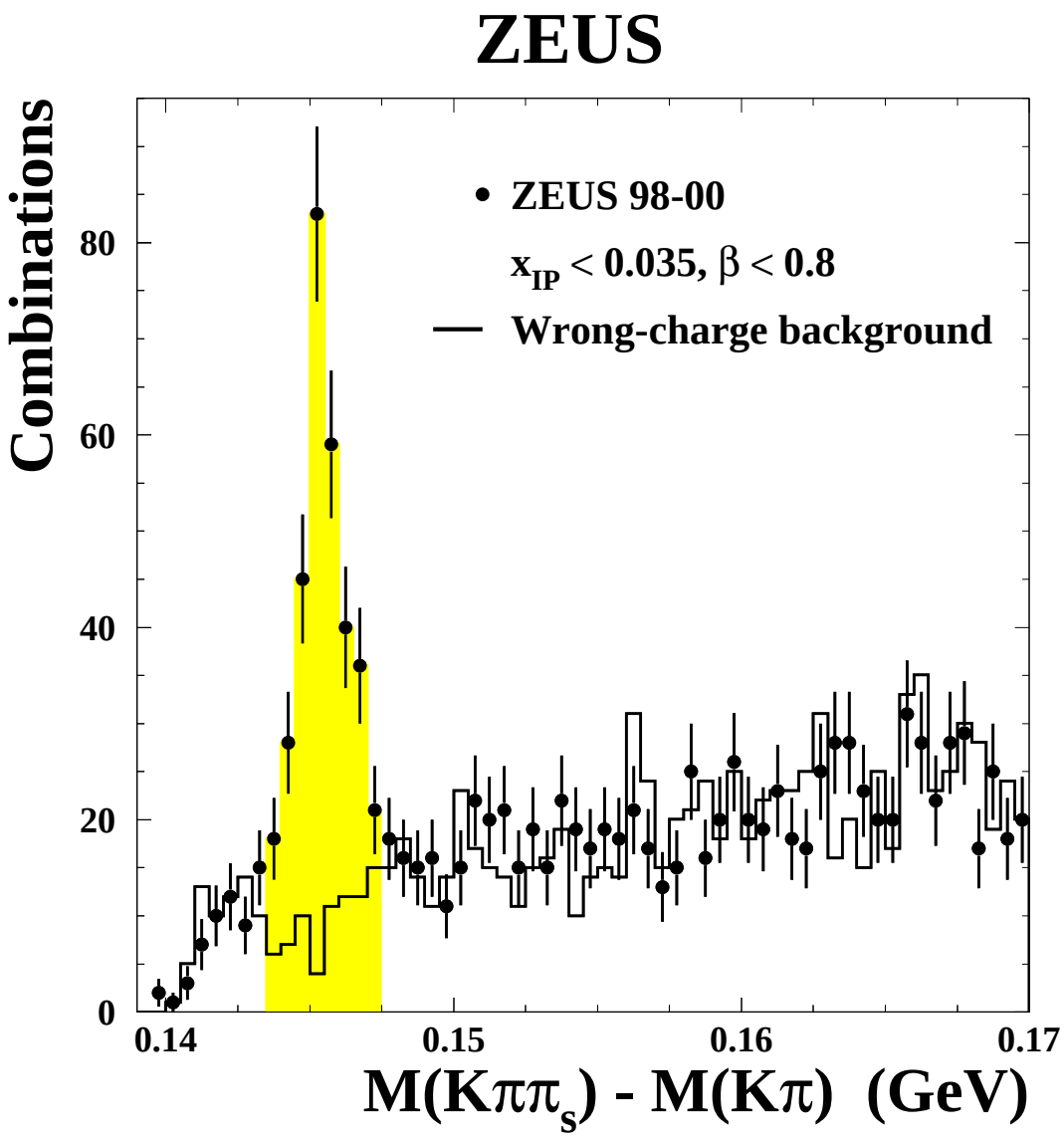

Figure 3: *The distribution of the mass difference, $\Delta M = M(K\pi\pi_s) - M(K\pi)$, for $D^{*\pm}$ candidates (dots) in events with $\eta_{\rm max} < 3$, $E_{\rm FPC} < 1.5\,GeV$, $x_{I\!P} < 0.035$ and $\beta < 0.8$. The histogram shows the ΔM distribution for wrong-charge combinations. Only $D^{*\pm}$ candidates from the shaded band were used for the differential cross-section measurements.*

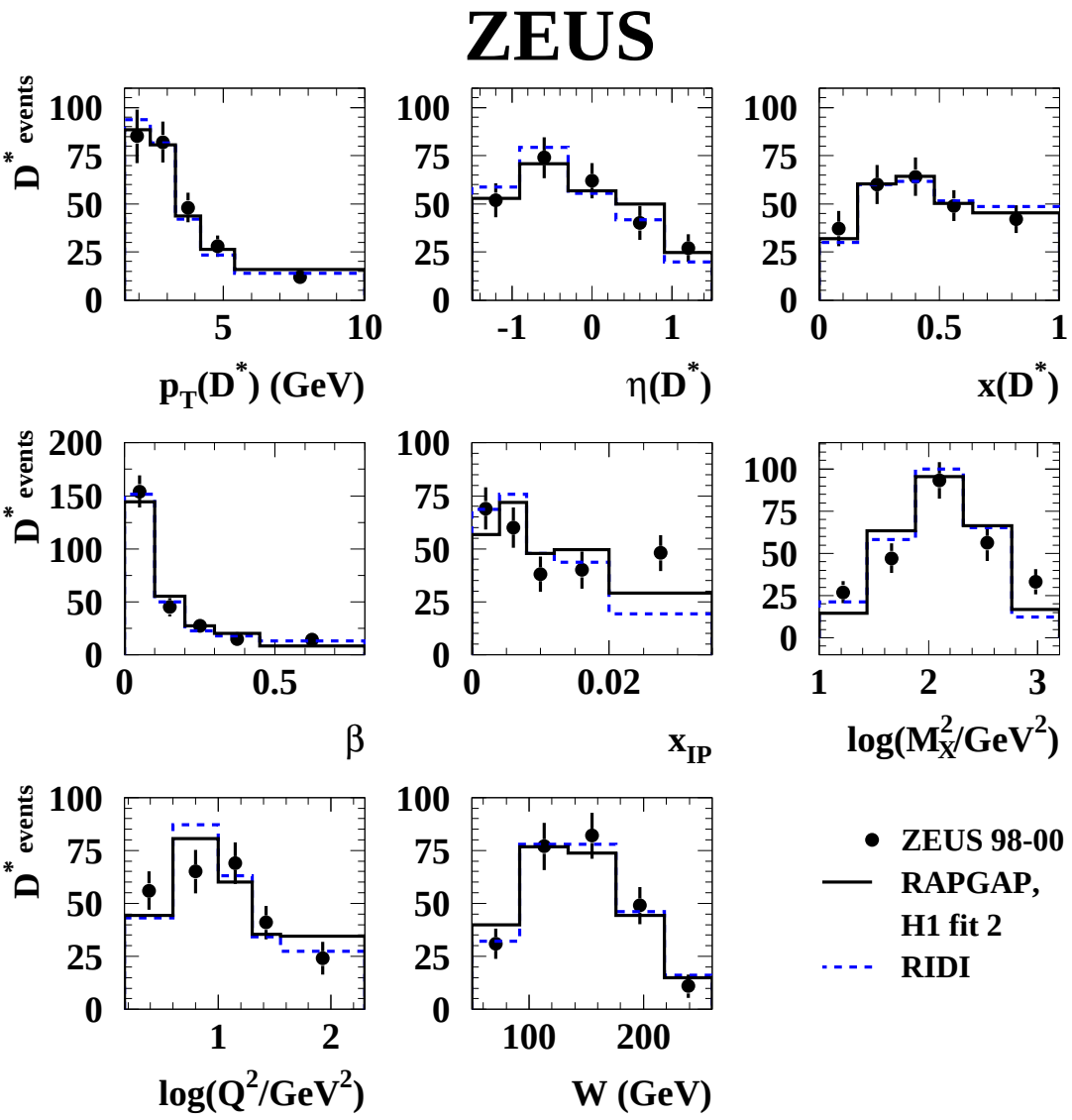

Figure 4: *Numbers of reconstructed $D^{*\pm}$ mesons (dots) in bins of $p_T(D^{*\pm})$, $\eta(D^{*\pm})$, $x(D^{*\pm})$, β, $x_{I\!P}$, $\log(M_X^2)$, $\log(Q^2)$ and W. The RAPGAP (solid histogram) and the mixed $c\bar{c}$ and $c\bar{c}g$ RIDI (dashed histogram) MC samples, normalized to the data, are shown for comparison.*

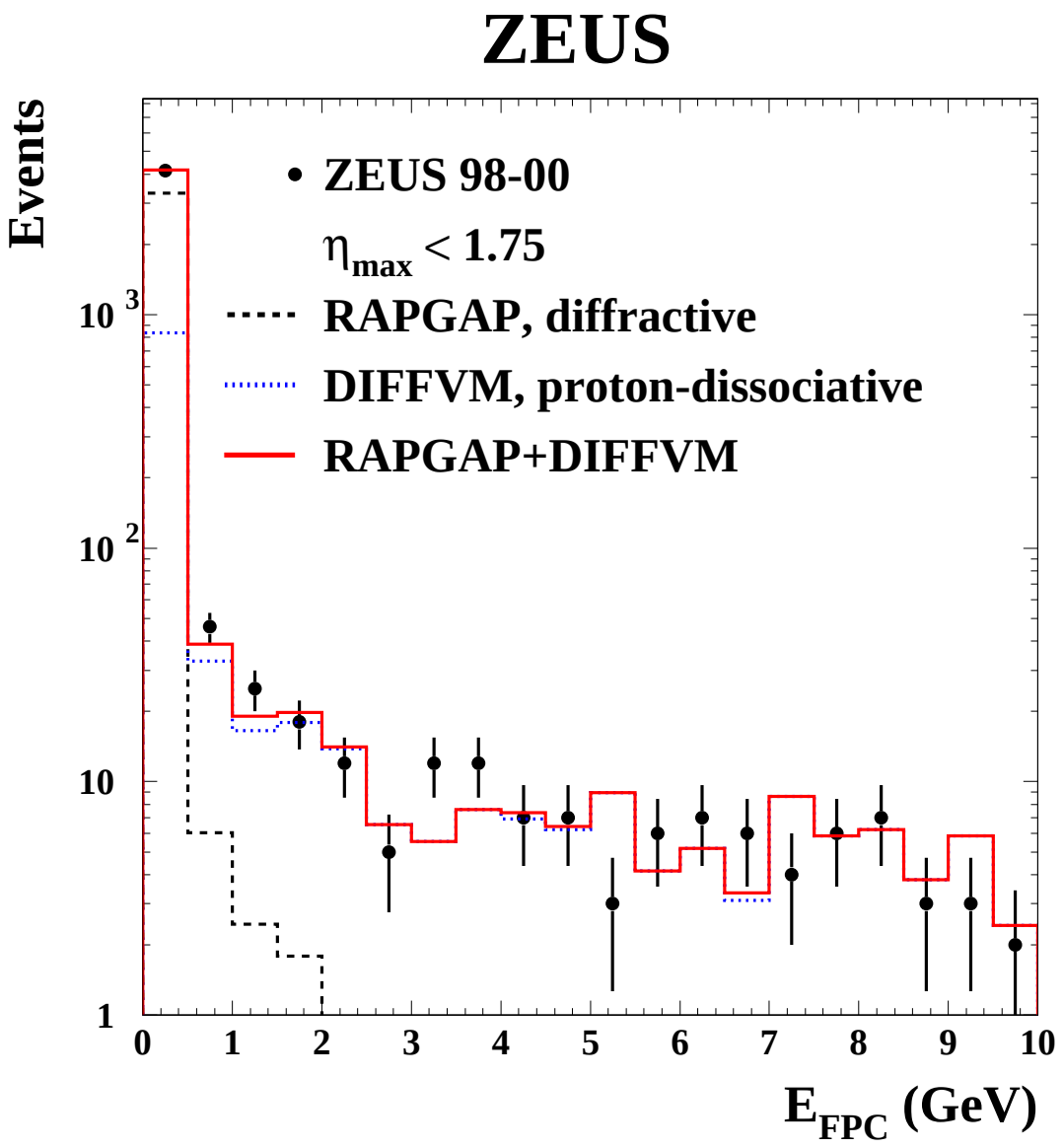

Figure 5: *The measured energy in the FPC for events with $\eta_{\max} < 1.75$ (dots). The dashed histogram is the single-diffractive RAPGAP MC sample and the dotted histogram is the proton-dissociative DIFFVM MC sample. The solid histogram is the sum of both diffractive and proton-dissociative MC samples normalised to the data.*

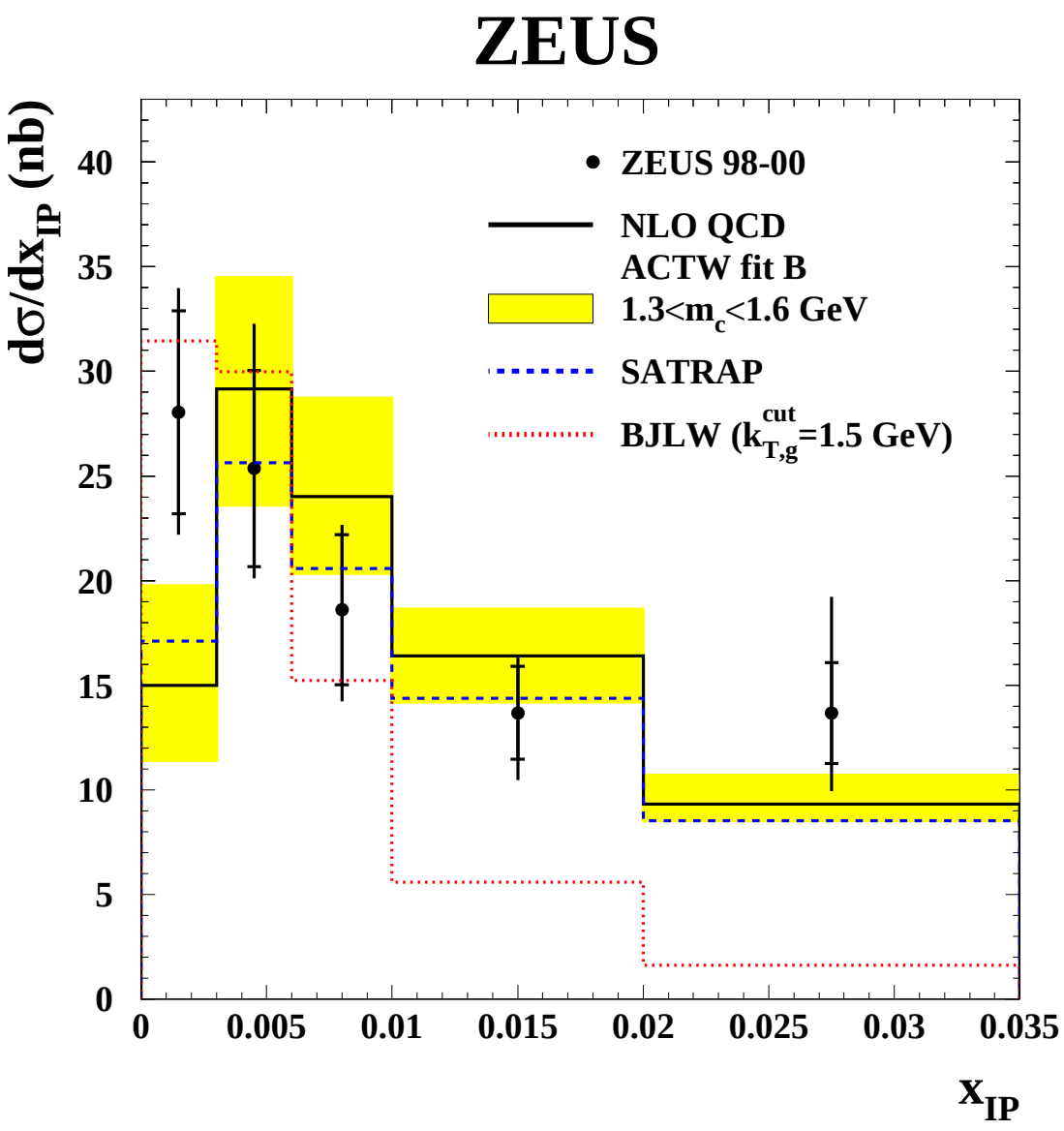

Figure 6: *Differential cross-section* $\mathrm{d}\sigma/\mathrm{d}x_{I\!P}$ *for diffractive* $D^{*\pm}$ *production for the data (dots) compared with the ACTW NLO (solid histogram), SATRAP (dashed histogram) and BJLW (dotted histogram) predictions. The shaded area shows the effect of varying the charm-quark mass in the ACTW NLO prediction. The inner error bars indicate the statistical uncertainties, while the outer ones correspond to statistical and systematic uncertainties added in quadrature. The overall normalisation uncertainties arising from the luminosity measurement (*$\pm 2.2\%$*), from the* $D^{*\pm}$ *and* D^0 *branching ratios (*$\pm 2.5\%$*) and from the proton-dissociative background subtraction (*$\pm 4.9\%$*) are not indicated.*

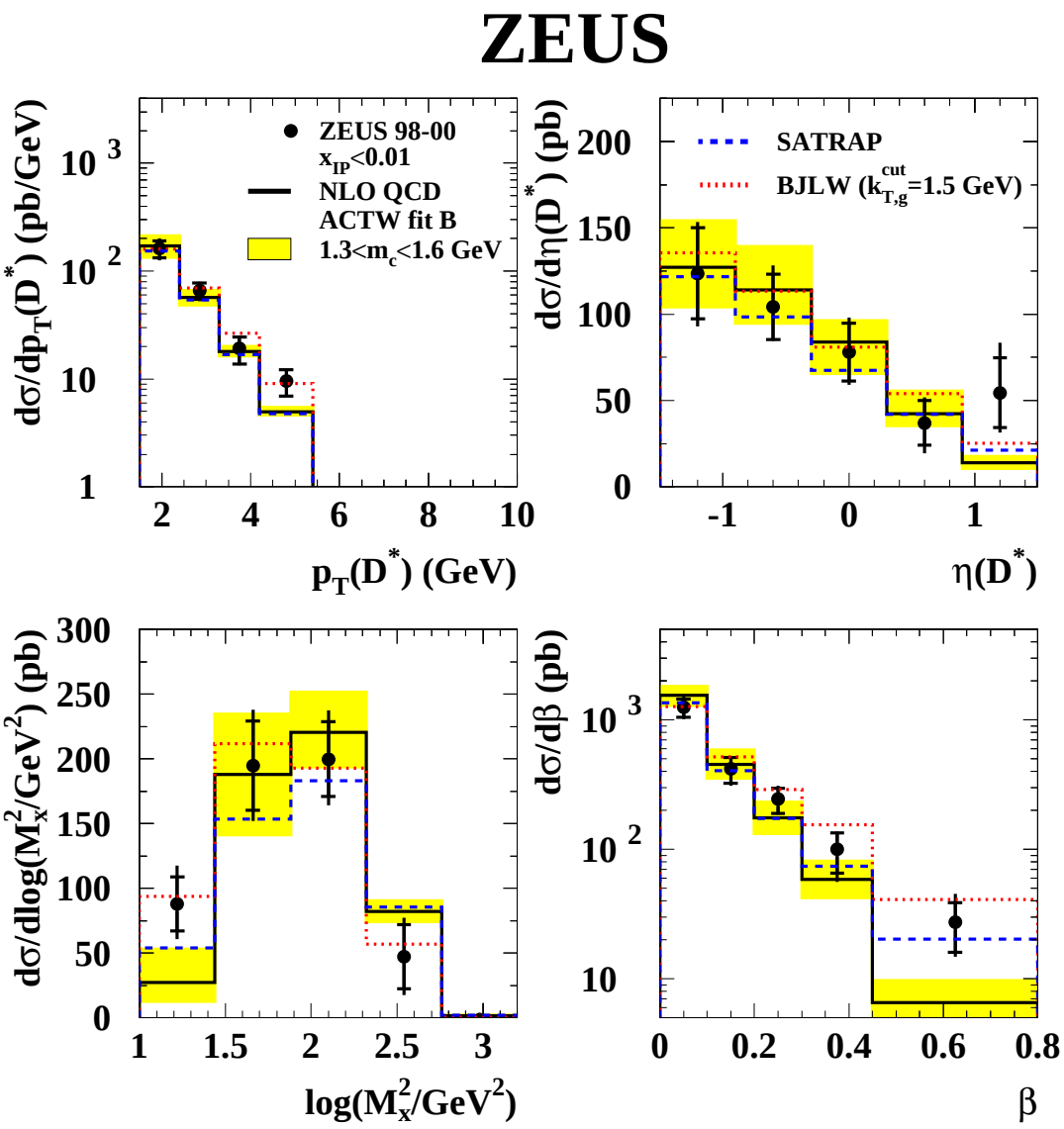

Figure 7: *Differential cross sections for diffractive $D^{*\pm}$ production with $x_{I\!P} < 0.01$ for the data (dots) compared with the ACTW NLO (solid histogram), SATRAP (dashed histogram) and BJLW (dotted histogram) predictions. The shaded area shows the effect of varying the charm quark-mass in the ACTW NLO prediction. The cross sections are shown as a function of $p_T(D^{*\pm})$, $\eta(D^{*\pm})$, $\log(M_X^2)$ and β. The inner error bars indicate the statistical uncertainties, while the outer ones correspond to statistical and systematic uncertainties added in quadrature. The overall normalisation uncertainties arising from the luminosity measurement ($\pm 2.2\%$), from the $D^{*\pm}$ and D^0 branching ratios ($\pm 2.5\%$) and from the proton-dissociative background subtraction ($\pm 4.9\%$) are not indicated.*

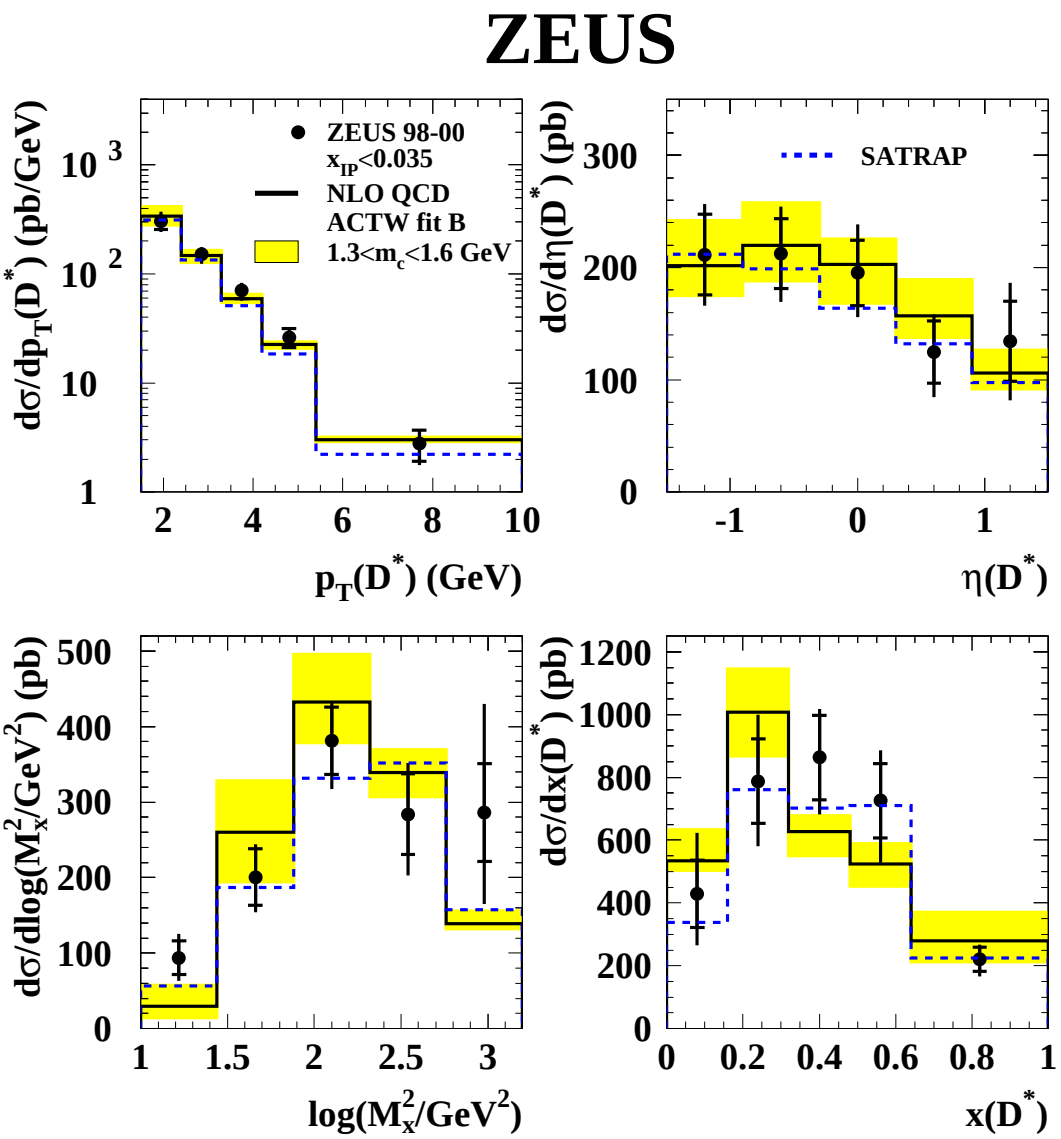

Figure 8: *Differential cross sections for diffractive $D^{*\pm}$ production with $x_{I\!P} < 0.035$ for the data (dots) compared with the ACTW NLO (solid histogram) and SATRAP (dashed histogram) predictions. The shaded area shows the effect of varying the charm-quark mass in the ACTW NLO prediction. The cross sections are shown as a function of $p_T(D^{*\pm})$, $\eta(D^{*\pm})$, $\log(M_X^2)$ and $x(D^{*\pm})$. The inner error bars indicate the statistical uncertainties, while the outer ones correspond to statistical and systematic uncertainties added in quadrature. The overall normalisation uncertainties arising from the luminosity measurement ($\pm 2.2\%$), from the $D^{*\pm}$ and D^0 branching ratios ($\pm 2.5\%$) and from the proton-dissociative background subtraction ($\pm 4.9\%$) are not indicated.*

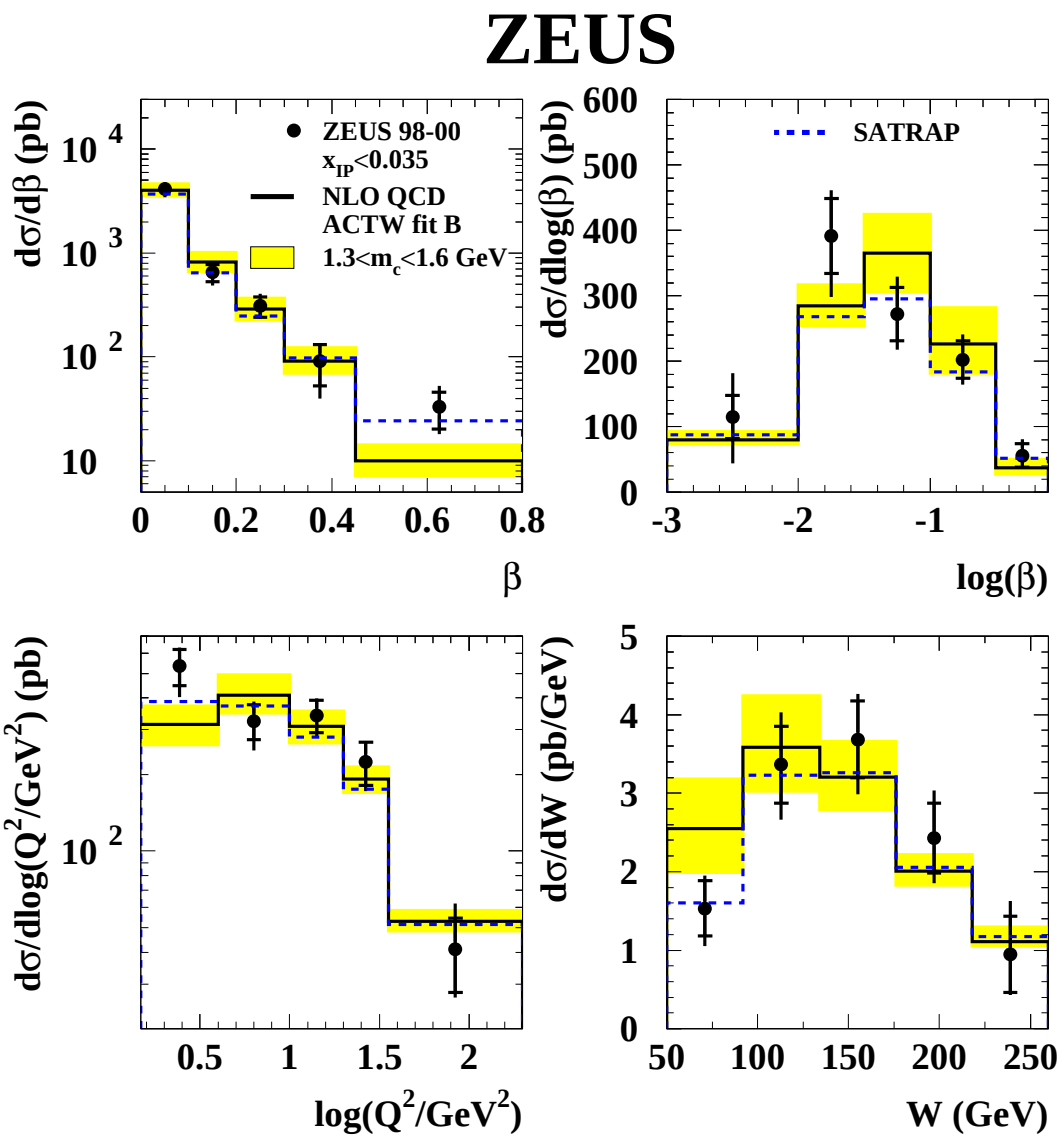

Figure 9: *Differential cross sections for diffractive $D^{*\pm}$ production with $x_{I\!P} < 0.035$ for the data (dots) compared with the ACTW NLO (solid histogram) and SATRAP (dashed histogram) predictions. The shaded area shows the effect of varying the charm-quark mass in the ACTW NLO prediction. The cross sections are shown as a function of β, $\log(\beta)$, $\log(Q^2)$ and W. The inner error bars indicate the statistical uncertainties, while the outer ones correspond to statistical and systematic uncertainties added in quadrature. The overall normalisation uncertainties arising from the luminosity measurement ($\pm 2.2\%$), from the $D^{*\pm}$ and D^0 branching ratios ($\pm 2.5\%$) and from the proton-dissociative background subtraction ($\pm 4.9\%$) are not indicated.*

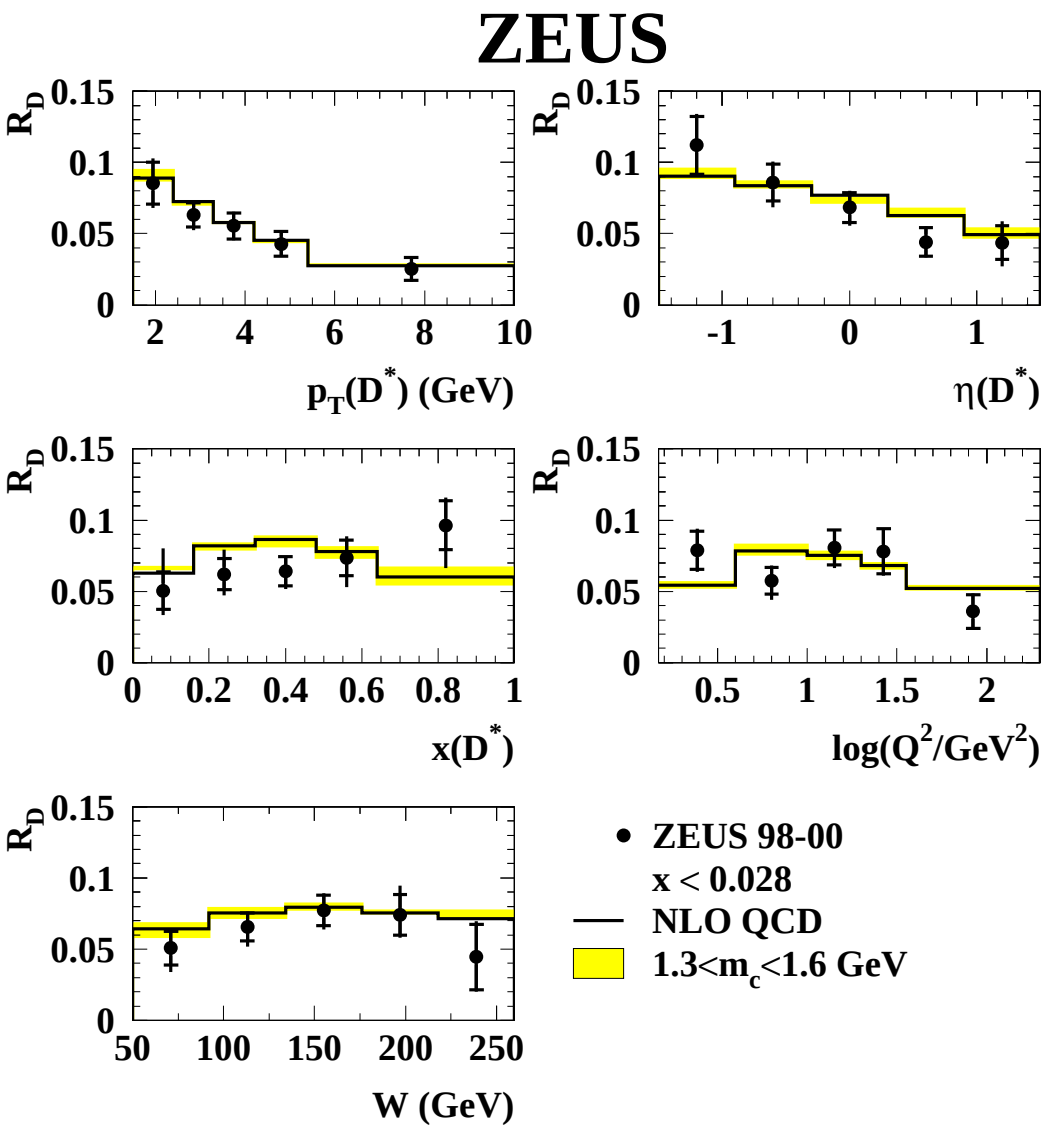

Figure 10: *The measured ratio of diffractively produced $D^{*\pm}$ mesons to inclusive $D^{*\pm}$ meson production (dots). The ratio is shown as a function of $p_T(D^{*\pm})$, $\eta(D^{*\pm})$, $x(D^{*\pm})$, $\log(Q^2)$ and W. The inner error bars indicate the statistical uncertainties, while the outer ones correspond to statistical and systematic uncertainties added in quadrature. The histogram corresponds to the NLO QCD prediction where the shaded area shows the effect of varying the charm-quark mass. The overall normalisation uncertainty arising from the proton-dissociative background subtraction ($\pm 4.9\%$) is not indicated.*

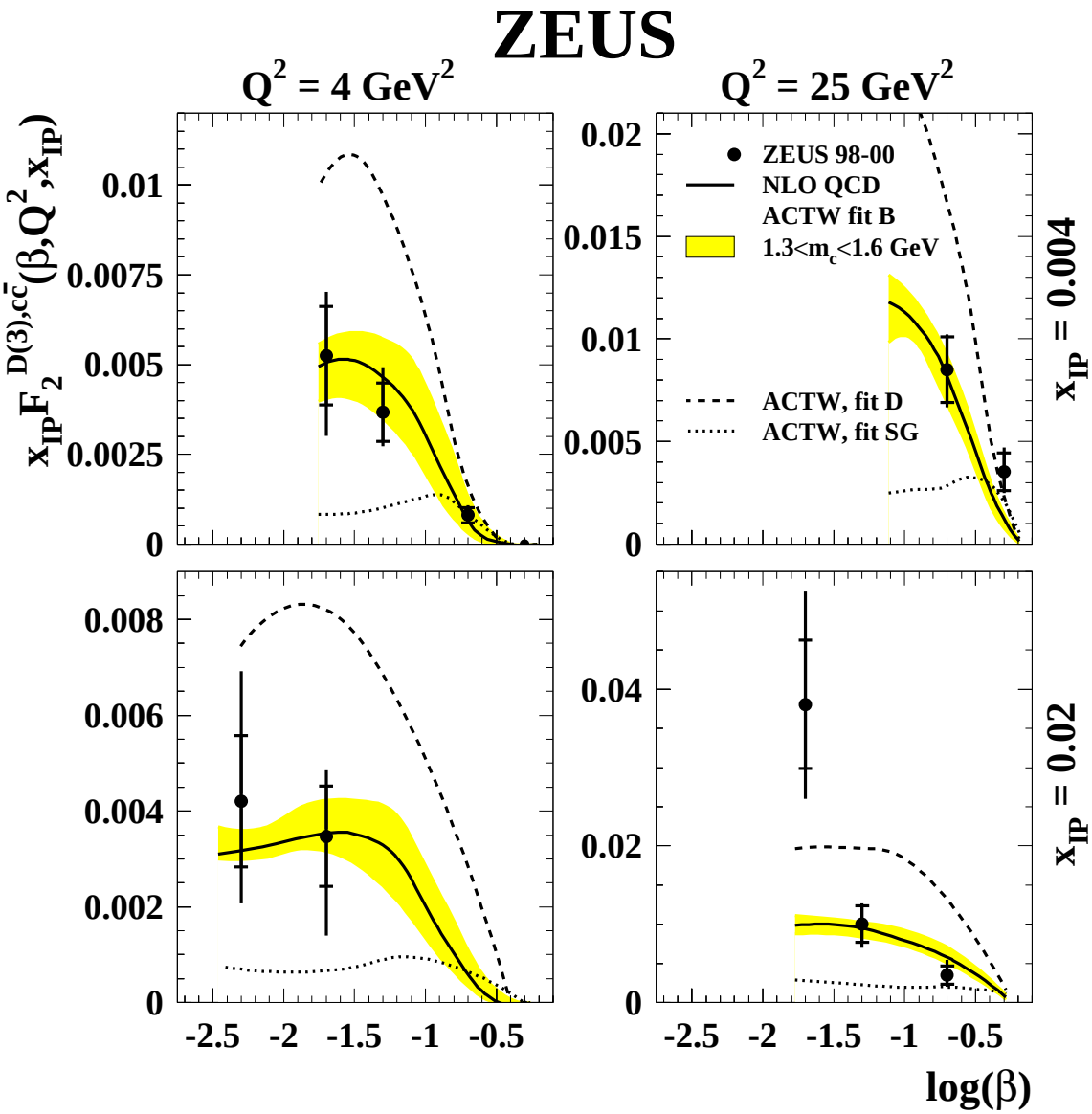

Figure 11: *The measured charm contribution to the diffractive structure function of the proton multiplied by $x_{I\!P}$, $x_{I\!P} F_2^{D(3),c\bar{c}}$, as a function of β for different values of Q^2 and $x_{I\!P}$ (dots). The inner error bars indicate the statistical uncertainties, while the outer ones correspond to statistical and systematic uncertainties added in quadrature. The overall normalisation uncertainties arising from the luminosity measurement (±2.2%), from the $D^{*\pm}$ and D^0 branching ratios (±2.5%) and from the proton-dissociative background subtraction (±4.9%) are not indicated. The curves correspond to the ACTW model prediction; the shaded area shows the effect of varying the charm-quark mass.*